

Contents lists available at ScienceDirect

Petroleum Science

journal homepage: www.keaipublishing.com/en/journals/petroleum-science



Original Paper

Hydrothermal carbon nanospheres as environmentally friendly, sustainable and versatile additives for water-based drilling fluids



Han-Yi Zhong ^{a, b, *}, Shu-Sen Li ^{a, b}, Da-Qi Li ^c, Jun-Bin Jin ^c, Chang-Zhi Chen ^{a, b}, Zheng-Song Qiu ^{a, b}, Wei-An Huang ^{a, b}

- ^a State Key Laboratory of Deep Oil and Gas, China University of Petroleum (East China), Qingdao, 266580, Shandong, China
- ^b School of Petroleum Engineering, China University of Petroleum (East China) Qingdao, 266580, Shandong, China
- ^c SINOPEC Research Institute of Petroleum Engineering Co., Ltd., Beijing, 102200, China

ARTICLE INFO

Article history: Received 24 September 2024 Received in revised form 15 March 2025 Accepted 17 March 2025 Available online 18 March 2025

Edited by Jia-Jia Fei

Keywords:
Water-based drilling fluid
Hydrothermal carbon nanosphere
Polymer degradation
Thermal stability
Radical scavenger
Sealing properties
Lubrication

ABSTRACT

In this study, hydrothermal carbon nanospheres (HCNs) were prepared by hydrothermal carbonization using glucose as the precursor, and introduced to improve the properties of water-based drilling fluid for the first time. The variation in rheological and filtration characteristics of water-based drilling fluid with varying concentrations of HCNs were compared between the cases before and after thermal aging. The results demonstrated that HCNs had little influence on the rheological properties of bentonite base mud, but could effectively reduce its filtration loss after thermal aging at 220 °C. For polymer-based drilling fluid, HCNs also exhibited minor influence on the rheology. The H-B model was the best fitting model for the rheological curves before thermal aging. After hot rolling at 220 °C, the viscosity retention rate increased from 29% to 63%-90% with addition of HCNs, and the filtration loss decreased by 78% with 1.0 w/v% HCNs. Meanwhile, the polymer-based drilling fluid with 0.5 w/v% HCNs maintained relatively stable rheology and low filtration loss after statically thermal aging at 200 °C for 96 h. For a bentonitefree water-based drilling fluid prepared mainly with modified natural polymers, the viscosity retention increased from 21% to 74% after hot rolling at 150 °C with 0.5 w/v% HCNs, and was further improved when HCNs and potassium formate were used in combination. The mechanism study revealed that, HCNs could trap dissolved oxygen, scavenge the free radicals and cross link with polymers, which prevented thermal oxidative degradation of polymers and improved the thermal stability of water-based drilling fluid. Meanwhile, HCNs could inhibit clay hydration and swelling in synergy with partially hydrolyzed polyacrylamide by physically sealing the micropores, contributing to shale formation stability. Furthermore, HCNs could effectively improve the lubrication and anti-wear performance of drilling fluid. This study indicated that HCNs could act as green, sustainable, and versatile additives in water-based drilling fluid.

© 2025 The Authors. Publishing services by Elsevier B.V. on behalf of KeAi Communications Co. Ltd. This is an open access article under the CC BY-NC-ND license (http://creativecommons.org/licenses/by-nc-nd/4.0/).

1. Introduction

Although stunning progress in renewable alternative energy resources has been made during the past decades, it is predicted that the hydrocarbon-based fuels including oil and gas are still the primary energy sources in the future (Rana et al., 2021). The high demand on oil and gas and increased depletion of surface reservoir around the world drive the petroleum industry to hunt for more

2012). Drilling fluids, as the blood of drilling engineering, play an important role in ensuring safe, efficient and successful drilling target. Drilling fluids have multifunction including circulating and transporting the drilling cuttings, stabilizing wellbore and balancing the formation pressure, cooling and lubricating the drill bit and transmission of hydrodynamic force (Aftab et al., 2017). Drilling fluids are generally sorted into water-based drilling fluid and oil-based drilling fluid. Because of high temperature stability, excellent shale hydration inhibition and lubricity, oil-based drilling

fluids are preferred in complicated and challenging formations,

challenging reservoirs such as deep/ultra-deep formations and unconventional shale oil/gas formations (Hassiba and Amani,

E-mail address: zhonghanyi@126.com (H.-Y. Zhong).

^{*} Corresponding author.

however, the relatively high cost and adverse effect on the environment restrict their wide use.

Water-based drilling fluid is typically consisted of bentonite, polymers, surfactants, inorganic salts and weighting materials. Various types of polymers are widely used in water-based drilling fluid to control the rheology, filtration loss, shale stability and lubricity. However, when complicated formation conditions are encountered, conventional water-based drilling fluids are inadequate to acquire satisfactory properties. For example, to maintain the wellbore stability of unconventional shale formations with nano-pores and extremely low permeability, suitable nanoparticles are essential to build an internal filter cake and thereby reduce the fluid invasion into the shale because the size of solids in conventional water-based drilling fluid is too large to plug the nano-pores (Sensoy et al., 2009). Another case is the extended reach well and horizontal well drilling. The coefficient of friction for a water-based drilling fluid typically ranges from 0.25 to 0.35 (Akaighe et al., 2023). The high friction and drag are the key factor limiting horizontal displacement. Although numerous lubricants have been developed to reduce the friction and torque, the performance of these lubricants at downhole elevated temperature environments is often inconsistent (Zhou et al., 2023). In addition, more and more deep and ultra-deep wells and geothermal wells with high temperature high pressure (HTHP) conditions have been drilled in recent years. Conventional water-based drilling fluids using biopolymers and their derivatives generally become unstable above 150 °C due to oxidative and hydrolytic processes (Ezell et al., 2010). Therefore, as the above extreme field environments are encountered more frequently than before, the oil and gas industry call for a new generation of high performance water-based drilling fluids, which can provide better drilling hydraulics, shale stabilization and lubrication, high-temperature rheology and filtration loss control similar to oil-based drilling fluids (Teherani et al., 2007), but at the same time to be environmentally friendly (Affede et al., 2023).

During the past decades, various types of additives have been employed to formulate efficient drilling fluid systems. Among these additives, nanoparticles, because of their ultrafine size, high surface area to volume ratio, and excellent thermal conductivity, have attracted much attention and been introduced into drilling fluids to achieve desirable properties, such as adjusting rheological and filtration properties, plugging the micro and nano-pores, enhancing thermal stability, thermal and electrical conductivities, and lubricity (Beg et al., 2019; Rafati et al., 2018). In addition, smart drilling fluids can be designed using specially-made nanoparticles to solve specific problems in the process of drilling (Murtaza et al., 2023)

It is worth noting that, carbon-based nanomaterials, mainly including graphenes and their derivatives, carbon nanotubes and fullerenes, exhibit extraordinary physical, mechanical, chemical and electronic properties, have been the research focus in recent years (Rana et al., 2021). For example, nano graphene provides superior lubricity and thermal stability to water-based drilling fluid (Taha and Lee, 2015). Being ultrathin and flexible, it is easy for graphene oxide to deform and plug various shapes and sizes of nanopore (Kamal et al., 2023). Wang et al. (2020) prepared graphene oxide and found that large and unbroken graphene oxide sheets could form a protective film. The small sheets could deform and seal micropores of shale. Halali et al. (2016) investigated the effect of carbon nanotubes on the properties of water-based drilling fluid. The results indicated that carbon nanotubes could maintain the thermal stability of biopolymers. The HTHP filtration loss was reduced by 93.3% and the thermal conductivity was enhanced by 12% with the addition of carbon nanotubes. Murtaza et al. (2023) incorporated graphite nanoparticles into water-based drilling fluid and found the addition of nanoparticles maintained the

stability of drilling fluids at HTHP conditions and resulted in a stable rheological profile. However, the preparation conditions of graphene oxide and carbon nanotube are demanding and complex, meanwhile their cost are relatively high, which limit their extensive application.

When biomass is dispersed in water and subjected to temperatures ranging from 180 to 280 °C under self-generated pressures, it experiences a series of complex reactions—such as hydrolysis. dehydration, decarboxylation, condensation, polymerization and aromatization (Ischia et al., 2022) -a process known as hydrothermal carbonization (Saha et al., 2019). This process produces a type of carbonaceous materials called hydrothermal carbon spheres, or hydrochars. These hydrochars, characterized by abundant oxygen-containing functional groups on their surface, exceptional chemical and thermal stability, adjustable sizes (ranging from hundreds of nanometers to a few micrometers) and structures, exhibit remarkable properties. They have shown potential in various research areas, including heavy metal ion adsorption, capacitive electrode materials, gas storage, and catalysts for organic synthesis reactions (Fang et al., 2022; Jaruwat et al., 2018). What is more, the HTC process is a "green synthesis" strategy without the need to use any hazardous solvents, which allows the production of hydrothermal carbon spheres to be an easy and scalable route (Titirici and Antonietti, 2010).

Among the biomass materials, glucose is the most abundant sugar unit and inexpensive saccharide available. It is the major product of acidic hydrolysis of lignocellulosic biomass and usually employed as a model for hydrothermal carbonization (Avdincak et al., 2012; Ischia et al., 2022). Therefore, in the present study. the hydrothermal carbon nanospheres (HCNs) were synthesized from glucose with HTC. The potential of HCNs in improving the properties of water-based drilling fluid was systematically studied for the first time. Firstly, the chemical properties and morphology of HCNs were analyzed using various techniques, including Fourier transform infrared (FT-IR) spectroscopy, Raman spectroscopy, X-ray diffraction (XRD), thermogravimetric analysis (TGA), scanning electron microscopy (SEM), and transmission electron microscopy (TEM). Then the effects of HCNs on the rheology, filtration loss, shale stabilization, and lubricity properties of water-based drilling fluid were investigated. Extensive laboratory measurements including rheological and filtration properties before and after dynamic thermal aging, long-term static thermal aging, shale linear swelling, modified filtration test, extreme pressure lubrication and four ball friction testing were carried out to validate the HCNs' performance. Especially, the improvement in thermal stability of water-based drilling fluid was probed from the aspects of dissolved oxygen scavenging, free radical quenching, and interactions with polymers. This study offers a comprehensive assessment of the benefits of HCNs employment in water-based drilling fluids.

2. Materials and methods

2.1. Materials

Glucose, hydrochloric acid, sodium hydroxide, ferrous sulfate heptahydrate (FeSO₄·7H₂O), hydrogen peroxide (H₂O₂, 30 w/w%), methyl violet (MV) and 5,5-dimethyl-1-pyrroline N-Oxide (DMPO), all of analytical grade, were obtained from Shanghai Aladdin Biochemical Technology Co., Ltd. A high temperature resistant synthetic polymer (HTSP) using for filtration control was generously provided by Drilling Specialties Company. Sodium bentonite was supplied by Shengli Oilfield Boyou Mud Technology Co., Ltd. The formulation of the bentonite-free water-based drilling fluid is detailed in Table 1.

Table 1Bentonite-free water-based drilling fluid formulation.

Component	Function Concentra		ion, g			
		Fluid 1#	Fluid 2#	Fluid 3#	Fluid 4#	
Fresh water	_	400	400	400	400	
Caustic soda	Adjusting pH value	0.8	0.8	0.8	0.8	
Sodium carbonate	Adjusting pH value	0.8	0.8	0.8	0.8	
Xanthan gum	Rheological regulator	1.2	1.2	1.2	1.2	
Modified starch	Filtration reducer	4	4	4	4	
Polyanionic cellulose with low viscosity (PAC-LV)	Filtration reducer	1.2	1.2	1.2	1.2	
Polyamine	Shale inhibitor	8	8	8	8	
Lubricant	Lubrication	8	8	8	8	
No. 1 calcium carbonate (average particle size = $44 \mu m$)	Temporary plugging agent	8	8	8	8	
No. 2 calcium carbonate (average particle size $= 6.5 \mu m$)	Temporary plugging agent	4	4	4	4	
HCOOK	Weighting material	_	_	300	300	
HCNs		_	2	_	2	

2.2. Synthesis and characterization of HCNs

In a typical HCNs synthesis procedure, glucose solution (10 w/v%) was poured into a Teflon-line autoclave with a filling degree of 80%. Subsequently the autoclave was put in an oven and aged at 180 °C for a predetermined time of 12 h. After reaching the setting reaction time, the cell was soaked in water and cooled down to room temperature. The solid liquid separation of the mixture in the autoclave was achieved by centrifugation at 10,000 rpm for 30 min. Then the obtained solid products were thoroughly washed with ethanol and deionized water for at least three cycles. Followed by drying in the oven at 80 °C for 24 h and grinding, tawny HCN powders were obtained (Fig. 1). The productivity of HCNs was 28%.

The chemical groups present in HCNs were identified using a Fourier transform infrared (FT-IR) spectrometer (Thermo Scientific Nicolet iS20, USA). Spectra were recorded with the KBr pellet

method, covering a wave number range from 4000–400 cm⁻¹. The crystal structures of the HCNs were analyzed using an X-ray diffractometer (X'pert PRO MPD, Panalytical, Netherlands) operating at 42 kV and 40 mA with Cu-K α radiation (1.5406 nm) at a scanning rate of 8 $^{\circ}$ /min, ranging from 5 $^{\circ}$ to 75 $^{\circ}$. The morphology of the HCNs was observed with field-emission scanning electron microscopy (FEI Nova nanoSEM 450, USA) and transmission electron microscopy (JEOL JEM-2100Plus, Japan). Surface chemical composition and state were characterized by X-ray photoelectron spectroscopy (XPS) (Thermo Scientific, USA) using an Al Kα radiation source with an energy of 1486.6 eV. Thermal stability was evaluated using a thermogravimetric analyzer (Netzsch STA 449F3, Germany), heating the sample from 30 to 1000 °C at a rate of 10 °C/min under a nitrogen atmosphere. Raman spectra were obtained with a Raman spectrometer (Horiba LabRAM HR Evolution, Japan) using a 532 nm excitation wavelength. Particle size distribution and zeta potential

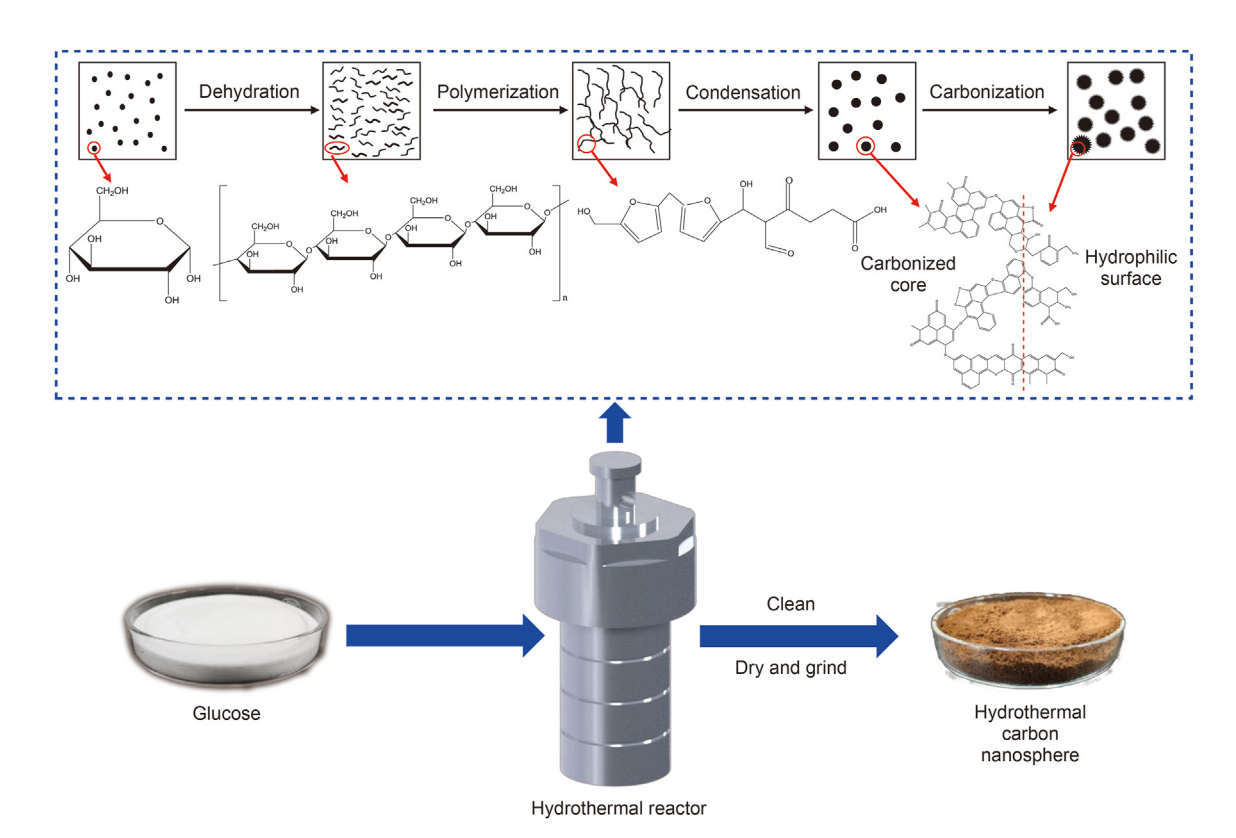


Fig. 1. Scheme of hydrothermal carbonization of glucose.

of HCNs suspensions at various pH levels were measured using a nanoparticle size and zeta potential analyzer (NanoBrook Omni, Brookhaven Instruments, USA).

2.3. Drilling fluid preparation

The bentonite base mud was prepared by mixing 16 g sodium bentonite, 0.8 g NaOH and 400 mL deionized water together in a Hamilton Beach mixer, followed by hydration for at least 24 h. Polymer-based drilling fluids were made by mixing HTSP (4 g) with the bentonite base mud (400 mL) for 30 min, then were allowed to incubate for 24 h. Bentonite-free water-based drilling fluids were prepared by sequentially adding various additives into the water with agitation, allowing each additive to be mixed for 10 min before adding the next. All fluids were mixed at a consistent agitation rate of 10,000 rpm to ensure uniformity.

2.4. Rheological properties measurement

HCNs with varying concentrations were mixed into the bentonite base mud and polymer-based drilling fluid, respectively. After agitation for 30 min, the rheological properties were measured immediately with an Anton Paar rheometer MCR 301 equipped with coaxial cylinders at 25 °C (outer radius is 38 mm, inner radius is 28 mm, height of the inner cylinder is 79 mm). Several rheological models are generally used to describe the rheological behavior of drilling fluids as follows:

Bingham mode :
$$\tau = \tau_0 + \mu_D \dot{\gamma}$$
 (1)

Power – law model :
$$\tau = K\dot{\gamma}^n$$
 (2)

Herschel – Bulkley (H – B) model :
$$\tau = \tau_0 + K\dot{\gamma}^n$$
 (3)

For the above three models, τ is the shear stress, and $\dot{\gamma}$ is the shear rate. For Bingham model, the fluids are described by a yield stress (τ_0) and plastic viscosity (μ_p). For Power-law model, it is defined by consistency coefficient (K) and flow behavior index (n). For H-B model, it is described by three parameters of τ_0 , K and n (Abu-Jdayil, 2011).

In order to evaluate the thermal stability, the prepared drilling fluid samples were dynamically aged at a setting temperature for 16 h. A ZNN-D6 six speed rotational viscometer (Qingdao Haitongda Special Instrument Co., Ltd) was used to measure the rheological parameters of the drilling fluid in both cases of before hot rolling (BHR) and after hot rolling (AHR). The steady dial reading at 600 and 300 RPM in viscometer were used to determine the apparent viscosity (AV), plastic viscosity (PV) and yield point (YP) by the following equations:

Apparent viscosity (AV) =
$$\Phi$$
600/2 (mPa·s) (4)

Plastic viscosity (PV) =
$$\Phi$$
600 $-\Phi$ 300 (mPa·s) (5)

Yield point (YP) =
$$(\Phi 300-PV)/2$$
 (Pa) (6)

The viscosity retention rate was calculated by the ratio of AV after hot rolling to AV before hot rolling. Generally, the viscosity retention rate above 50% suggested that testing fluid can withstand the temperature and meet the thermal stability requirement (Howard and Downs, 2015).

2.5. Filtration loss measurement and filter cake morphology observation

Before the filtration loss measurement, the drilling fluid was agitated by the Hamilton Beach mixer for 10 min to reach adequate dispersion. Then the API filtration loss volume was monitored with a standard medium pressure filter press apparatus (ZNS-2, Qingdao Haitongda Special Instrument Co., Ltd) with 0.7 MPa differential pressure at 25 °C. After collecting the filtrate with a graduate cylinder for 30 min, the fresh filter cake was obtained and its thickness was measured using a Vernier caliper. To preserve the original structure of the mud cake, it was rapidly frozen in liquid nitrogen for 1 h, then transferred to a lyophilizer and dried at $-50\,^{\circ}\mathrm{C}$. Following the drying process, the morphology of the filter cake was analyzed using SEM.

2.6. Soluble oxygen measurement

The dissolved oxygen content can be used to monitor the performance of antioxidant. In this study, the dissolved oxygen content of drilling fluid before and after dynamical aging was measured using a dissolved oxygen meter (Multi 3510 IDS SET 4, WTW, Germany). For the case of after dynamic aging, the aging cell was firstly cooled to ambient temperature. At the moment the cover was opened, the aging cell was quickly sealed with a plastic film to avoid the contact between the drilling fluid and air. Then the probe of the dissolved oxygen tester was passed through the plastic film. The dissolved oxygen content in the drilling fluid was determined (Fig. 2). The sensitivity of the probe was $\pm 0.5\%$ in liquid phase.

2.7. Ultraviolet spectrophotometry

The reaction between oxygen and residual initiators in commercial polymer products results in the formation of hydroxyl radicals, which are capable of attacking the backbone of polymers (Ash et al., 1983; Song et al., 2020). Hydroxyl radicals (·OH) are high reactive and can react with several hundred organic molecules without selectivity (Lankone et al., 2020). Scavenging the hydroxyl radicals can prevent the degradation of polymers and maintain the thermal stability.

Due to their short life and high reactivity, an indirect UV-Vis spectroscopy method was utilized to quantify the hydroxyl radicals. Methyl violet has the maximum absorbance at 582 nm. A typical Fenton reaction was performed to generate highly reactive hydroxyl radicals, which can decolorize methyl violet by oxidation reaction at pH 3.5, resulting in the reduction of absorbance.



Fig. 2. Scheme of soluble oxygen concentration measurement.

Therefore, changes in absorbance can indirectly indicate the amount of hydroxyl radicals generated.

Firstly, the variation of absorbance as a function of MV concentration was calibrated (Fig. 3). HCNs aqueous suspension with varying concentrations (0.4 mL) was prepared and transferred into a quartz tube. Followed by addition of 0.4 mL of 1.0 mM FeSO₄ solution, 4.0 mM $\rm H_2O_2$ solution, Tri-HCl buffer solution (pH = 3.7) and 2.0 mL of deionized water respectively, the absorbance ($A_{\rm experiment}$) was detected with UV1750 UV—visible spectrophotometer (SHIMADZU, Japan) after the reaction of mixture solution for 5 min. The absorbance of control group ($A_{\rm control}$) was detected using equal volume of deionized water to replace HCNs suspension. The absorbance of blank group ($A_{\rm blank}$) was determined using just 4.0 mL of MV solution (0.2 mM). The hydroxyl radicals scavenging rate was calculated as follows (Chen et al., 2023):

Scavenging rate =
$$(A_{\text{experiment}} - A_{\text{blank}}) / (A_{\text{control}} - A_{\text{blank}}) \times 100\%$$
 (7)

2.8. Electron paramagnetic resonance (EPR)

Except the above UV-Vis spectroscopy method to indirectly detect the concentration of hydroxyl radicals, another method using electron paramagnetic resonance was also used to directly quantify the concentration of hydroxyl radicals. Because hydroxyl radicals are short lived ($\approx 10^{-9}$ s), a spin-trap agent DMPO was used to react with the short-lived hydroxyl radicals and form relatively stable and longer-lived radical adducts that can be directly detected by EPR (Mittag et al., 2022). For the EPR measurement, $20 \mu L 5 \text{ mM}$ FeSO₄, 20 μ L 0.5 M DMPO, 20 μ L 0.05 M hydrogen peroxide, 40 μ L HCNs suspension and 300 µL deionized water were mixed and initiated the reaction. After mixing, 100 µL sample solution was transferred into a capillary (inner diameter 0.9-1.0 mm), then the capillary was placed in a paramagnetic quartz tube (inner diameter 4 mm) for EPR detection. The EPR spectrum was recorded using an EPR spectrometer (EMXnano, Bruker, Germany). Measurements were carried out under the following conditions: center field 3420.00 Guass, sweep width 100.0 Guass, frequency 9.625 GHz, power 3.162 mW, modulation frequency 100.00 kHz, sweep time 25.02 s, time const 1.28 ms, and temperature 20 °C. The hydroxyl radicals scavenging rate I was calculated as follows:

$$I = (h_0 - h_x)/h_0 \times 100\% \tag{8}$$

Here h_0 is the measured value of EPR spectrum signal intensity in the control sample (the second characteristic peak height); h_x is the measured value of EPR signal intensity in the sample (the second characteristic peak height).

2.9. Cryo-scanning electron microscopy (Cryo-SEM) observation

HTSP solution (1 w/v%) containing 0.5 w/v% HCNs and 0.1 w/v% NaOH was mixed and dynamically aged at 180 °C for 16 h. The morphology and structural changes of HTSP and HCNs before and after aging were imaged by the cryo-SEM and compared. Firstly, the sample was stuck on the conductive carbon glue and plunged into slushed nitrogen for 30 s to obtain a rapid freezing. The sample was then moved to the sample preparation chamber using a low-temperature freezing transport system. After sublimation at $-90\,^{\circ}\text{C}$ for 10 min, the sample was gold-coated by sputtering at a current of 10 mA for 60 s. The coated samples were analyzed with a field emission scanning electron microscope (Regulus8220, Hitachi High-tech Group) at an acceleration voltage of 5 kV, with the cold

stage maintained at −140 °C using liquid nitrogen.

2.10. Structure characterization of HCNs after thermal aging

HCNs aqueous suspension (1 w/v%, pH = 10) was transferred into a polytetrafluoroethylene cells with fitting degree of 80% and thermally aged at 200 °C for 16 h. Followed by cooling, centrifugation, washing and drying, the remaining HCN solids were collected. The structure variation of HCNs before and after thermal aging was characterized with 13 C nuclear magnetic resonance (13 C-NMR), Raman spectra and XPS.

2.11. Shale stabilization properties

To evaluate the clay hydration and swelling inhibitive properties, linear swelling test was performed and referred to our previous work (Zhong et al., 2020). The difference is that calcium bentonite was used in this experiment. A modified API filtration test was used to evaluate the sealing properties of HCNs (Fig. 4). Initially, 4.0 w/v% calcium bentonite suspension was filtered through the API filter paper under pressure difference of 0.7 MPa at room temperature for 30 min. When the test was finished, the pressure was relived and the filtration cell was open. The remaining calcium bentonite suspension in the filtration cell was gently extracted to avoid destruction of the filter cake. Then a testing fluid like deionized water or HCNs suspension was injected into the cell and the filtration loss volume was recorded again under the same pressure difference for 30 min. In the second round of filtration process, the filtration medium was mainly the formed filter cake, which has a much lower pore size than filter paper. After the test, the filter cake was carefully taken out and its thickness was determined by a vernier caliper. The permeability of the filter cake was calculated according to Darcy's law. Then the filter cake was put in liquid nitrogen for 1 h, followed by transferring into a freeze dryer for further drying. The morphologies of the dried filter cake were examined by SEM.

2.12. Lubrication properties evaluation

The extreme pressure lubricity coefficient of the polymer-based drilling fluid in the presence of varying content of HCNs was determined by an EP lubricity tester according to the recommended API standard. Meanwhile, MRS-100 Hydraulic four-ball friction and wear testing machine was adopted to evaluate the lubrication and

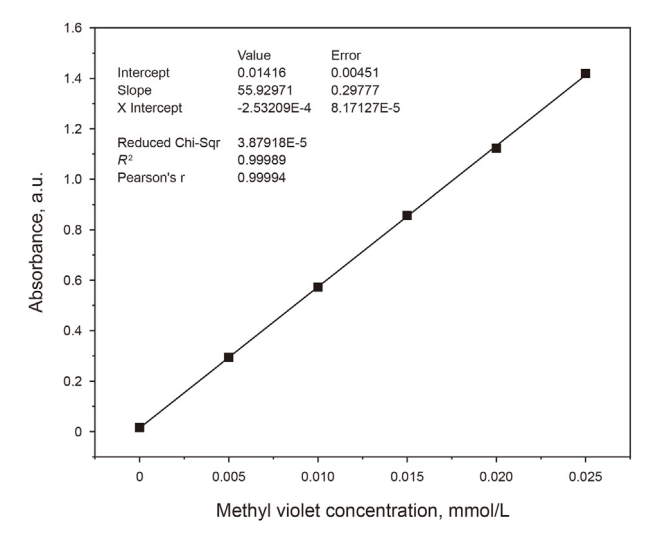


Fig. 3. Standard curve calibration.

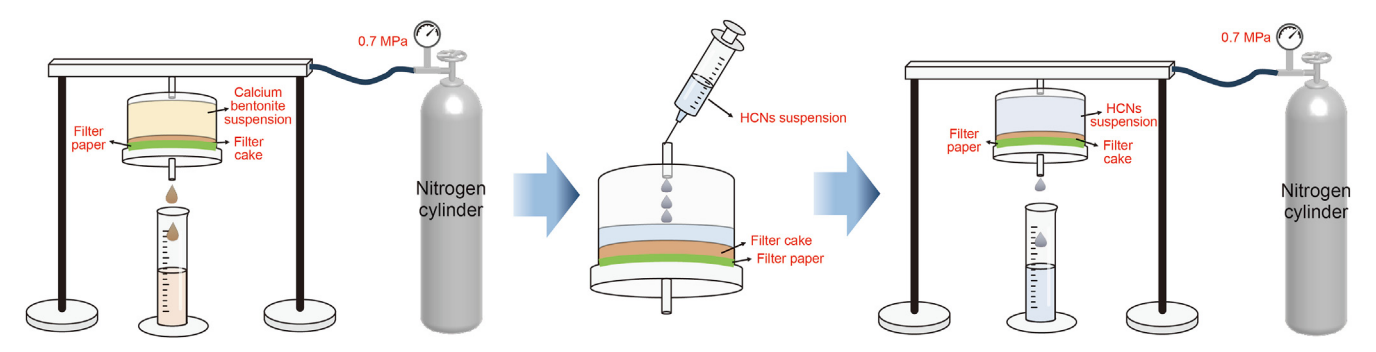


Fig. 4. Scheme of modified API filtration test.

anti-wear properties of HCNs, following the Standard of the Petrochemical Industry of the People's Republic of China "Determination Method for Wear Resistance of Lubricating Oil" (Four Ball Machine Method) (SH/T 0189–92) with testing pressure of 147 N, rotation speed of 1200 r/min, testing temperature of 25 °C and testing duration of 60 min. After the test, the wear scar of the bottom three balls was observed by a Zeiss Stemi 508 stereomicroscope.

3. Results and discussion

3.1. Characterization of HCNs

3.1.1. FT-IR

The FT-IR spectrum of HCNs is presented in Fig. 5(a). The band at $3421~{\rm cm}^{-1}$ is indicative of O–H (hydroxyl or carboxyl) stretching vibrations. The bands at $2973~{\rm and}~2909~{\rm cm}^{-1}$ correspond to C–H

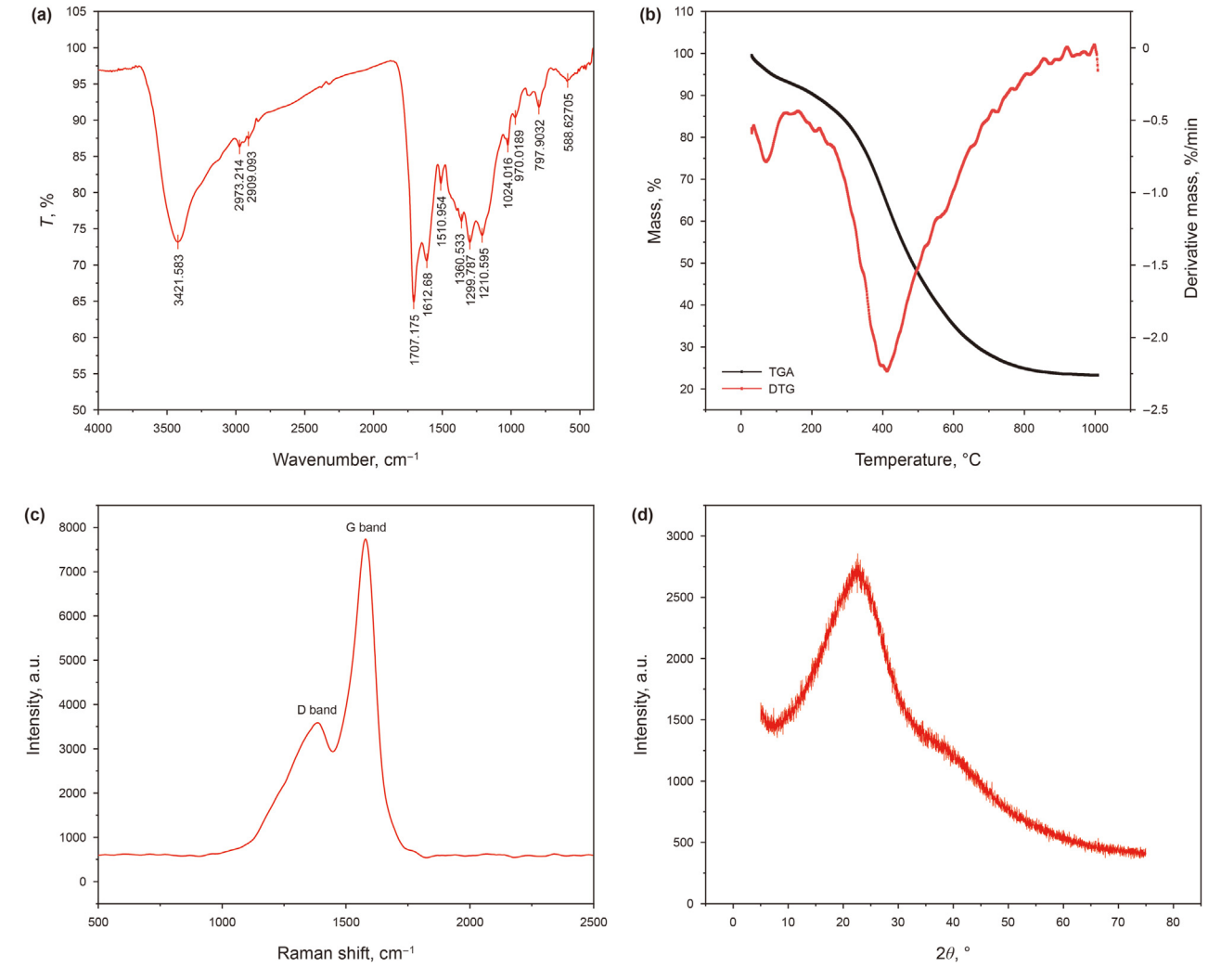


Fig. 5. Structure characterization of HCNs: (a) FT-IR, (b) TGA, (c) Raman spectrum and (d) XRD.

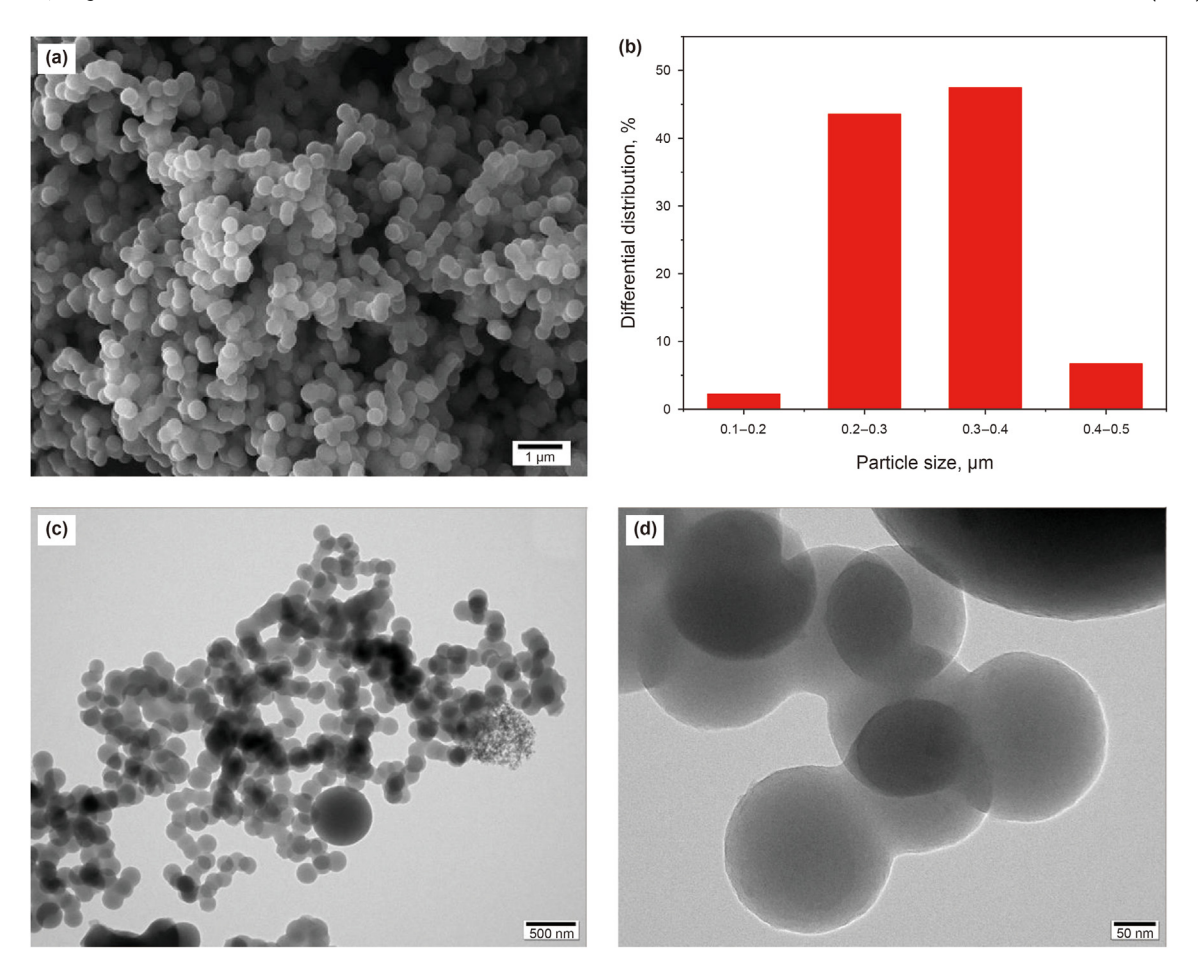


Fig. 6. SEM and TEM images of HCNs.

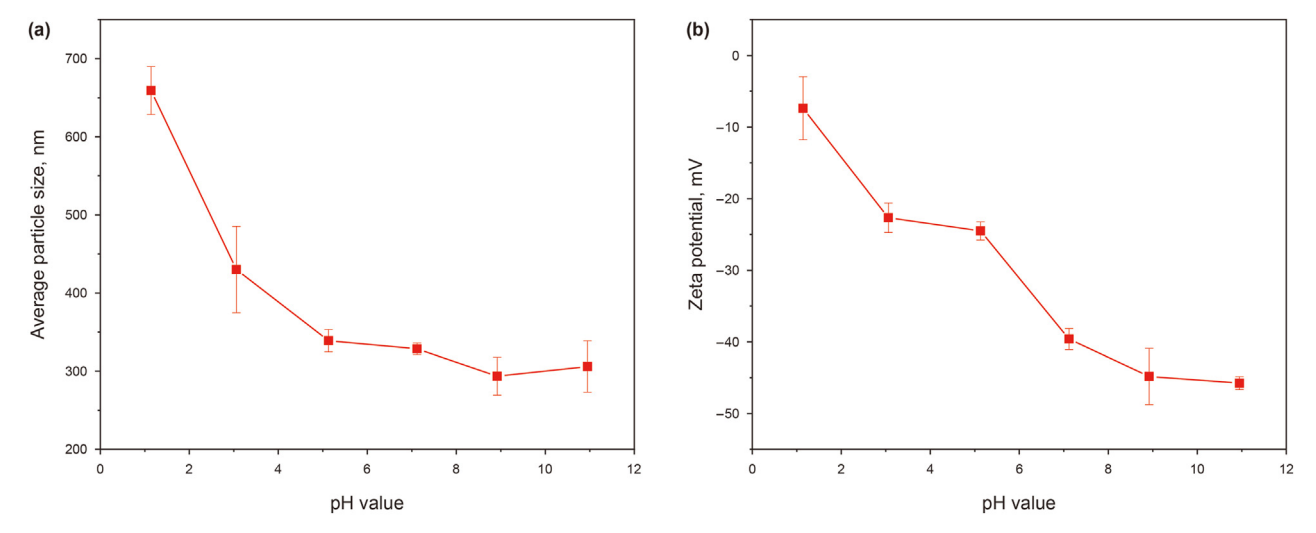


Fig. 7. (a) Variation of average particle size and (b) zeta potential of HCNs as a function of pH value.

stretching vibrations. The bands at 1707 and 1612 cm $^{-1}$ are attributed to the C=O stretching vibration of the aromatic carboxyl group (CH–C=O) and C=C stretching vibrations, respectively, supporting the concept of biomass aromatization during hydrothermal treatment (Wang et al., 2018). Characteristic bands at 1211 and 1024 cm $^{-1}$ are due to the asymmetric stretching of C–O–C and

bending vibrations of O–H, respectively. The band at 798 cm⁻¹ is associated with aromatic C–H out-of-plane bending vibrations (Supriya et al., 2015). These observations suggest that the abundant hydrophilic functional groups, including hydroxyl, carboxylic, and carbonyl groups, contribute to the high dispersion stability of HCNs in aqueous solutions.

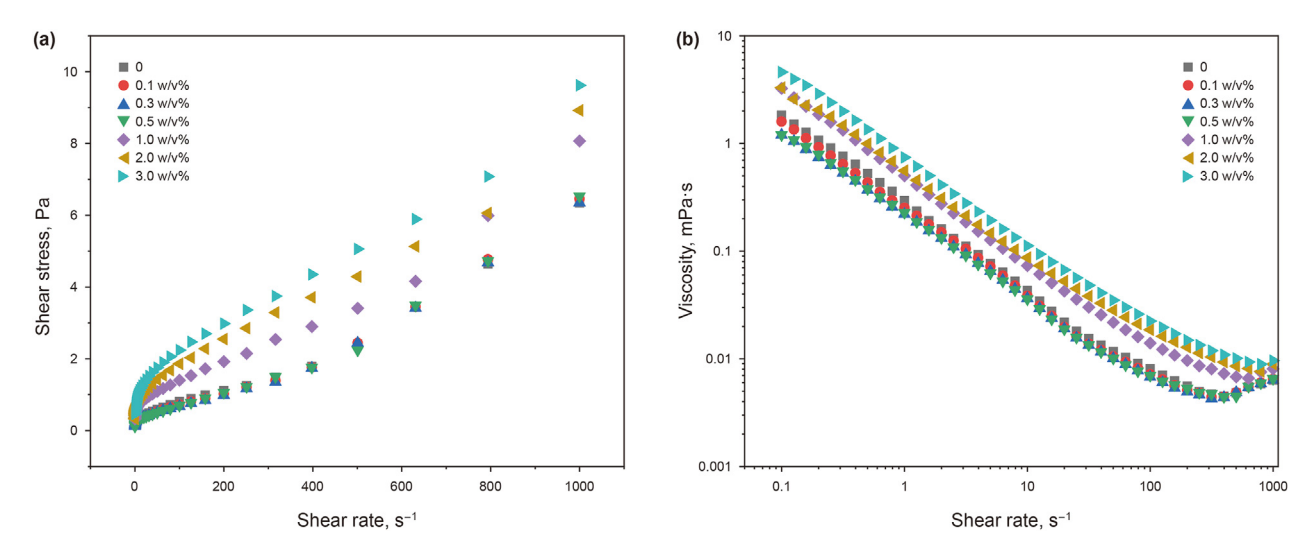


Fig. 8. (a) Shear stress and (b) viscosity versus shear rate for bentonite base mud with varying concentrations of HCNs.

Table 2 The rheological parameters and R^2 of three models for bentonite base mud at different concentrations of HCNs.

HCNs concentration, w/v%	Bingham model			Power-law model			H-B model			
	η _P , Pa·s	τ_0 , Pa	R^2	K, Pa·s ⁿ	n	R^2	τ_0 , Pa	K, Pa·s ⁿ	n	R^2
0	0.0054	0.247	0.972	0.2728	0.2929	0.8485	0.3533	4.3473×10^{-4}	1.3772	0.9916
0.1	0.0055	0.1986	0.9687	0.2396	0.3077	0.848	0.3164	3.2525×10^{-4}	1.4243	0.9934
0.3	0.0054	0.1699	0.9703	0.2055	0.3327	0.8763	0.2835	3.6127×10^{-4}	1.4072	0.9935
0.5	0.0055	0.171	0.9679	0.209	0.3313	0.8714	0.2896	3.3241×10^{-4}	1.4222	0.9918
1	0.0068	0.5412	0.9794	0.4772	0.2791	0.8988	0.5912	0.0033	1.1106	0.9812
2	0.0077	0.7065	0.9751	0.5382	0.3001	0.9378	0.6002	0.0214	0.8451	0.9799
3	0.0084	0.94	0.9766	0.73	0.2745	0.9305	0.7710	0.0336	0.7924	0.986

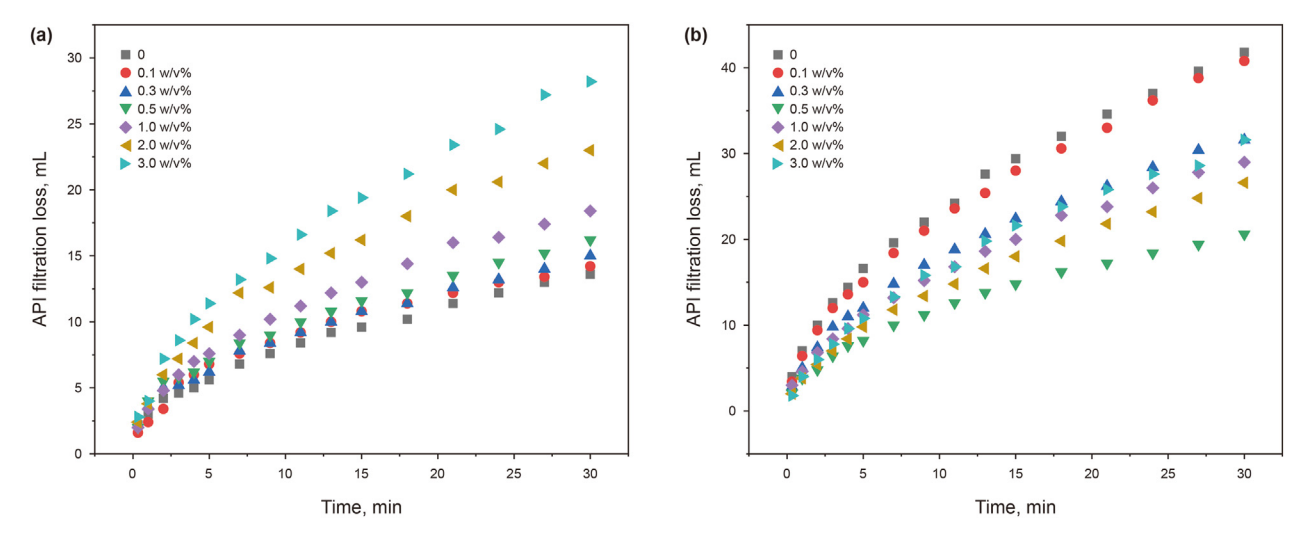


Fig. 9. Effect of HCNs on the API filtration properties (a) before and (b) after thermal aging at 220 °C.

3.1.2. TGA

The thermal decomposition behavior of HCNs was characterized and shown in Fig. 5(b). The weight loss between 30 and 100 °C was ascribed to the loss of the adsorbed water. The weight loss before 300 °C was associated with the degradation of oxygen-containing functional groups. At temperature between 300 and 600 °C, a single-step degradation corresponding to the majority of the weight loss of 48% was observed, demonstrating the decomposition of the hydroxymethylfurfural (HMF) oligomers in the HCNs (Inada et al., 2017). The maximum weight loss rate of HCNs occurred at 412 °C.

3.1.3. Raman spectrum and XRD

As shown in Fig. 5(c), the Raman spectrum of HCNs shows two characteristic peaks at 1387 (D band) and 1579 cm⁻¹ (G band). The D band corresponds to the breathing modes of the rings or defects in the graphite lattice, while the G band is associated with the vibrational modes of sp² carbon atoms in defect-free graphene sheets (Yu et al., 2023). The peak intensity ratio (ID/IG) normally indicates the level of disorder of the graphitic materials. The ID/IG value of HCNs is 0.47, which is consistent with previous study, also verifies the low graphitic degree of HCNs (Ischia et al., 2022). The

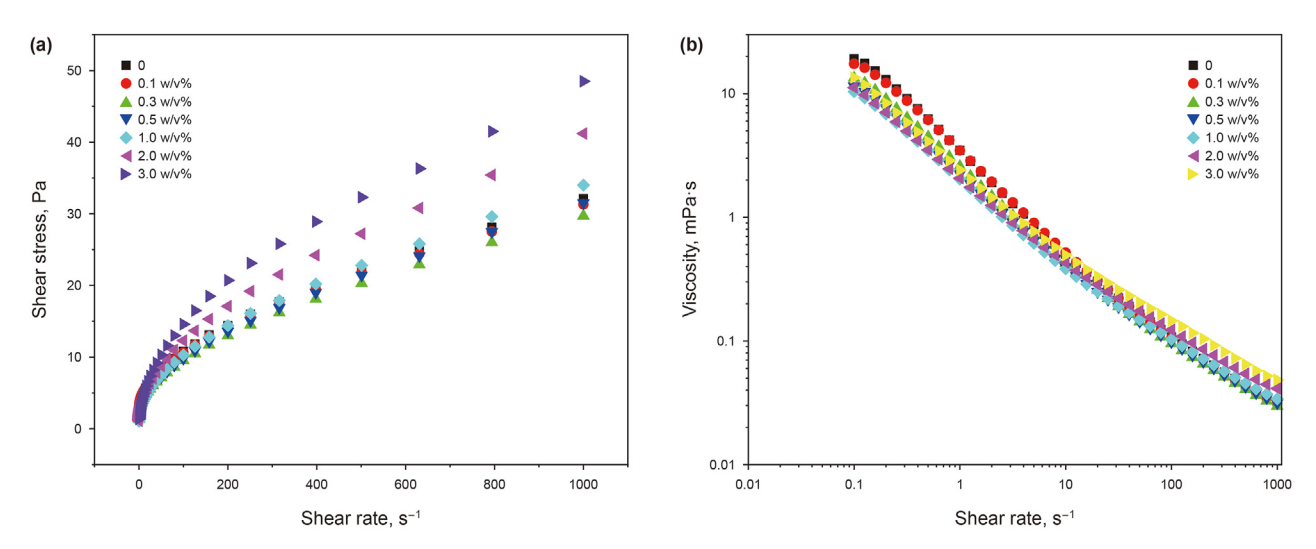


Fig. 10. (a) Shear stress and (b) viscosity versus shear rate for polymer-based drilling fluid with varying concentrations of HCNs.

Table 3The rheological parameters of various models for water-based drilling fluid with varying content of HCNs.

HCNs concentration, w/v%	Bingham model			Power-law model			H-B mode	H-B model			
	η _P , Pa·s	$ au_0$, Pa	R^2	K, Pa·s ⁿ	n	R^2	$ au_0$, Pa	K, Pa·s ⁿ	n	R^2	
0	0.0318	4.7453	0.9306	3.3353	0.2713	0.9522	2.6145	0.6486	0.5497	0.9989	
0.1	0.031	4.7441	0.9265	3.2783	0.2745	0.963	2.5611	0.6844	0.5381	0.9982	
0.3	0.03	3.8651	0.9305	2.5056	0.3066	0.9697	1.8424	0.6172	0.5488	0.9990	
0.5	0.0324	3.6587	0.9305	2.2135	0.3356	0.974	1.4817	0.6631	0.5493	0.9994	
1	0.0353	3.583	0.9323	2.0372	0.3609	0.9779	1.2653	0.6969	0.5545	0.9995	
2	0.0428	4.0103	0.9325	2.1489	0.3827	0.98	1.2082	0.8405	0.5555	0.9994	
3	0.0506	4.7413	0.9276	2.5122	0.3844	0.9772	1.2748	1.0640	0.5460	0.9995	

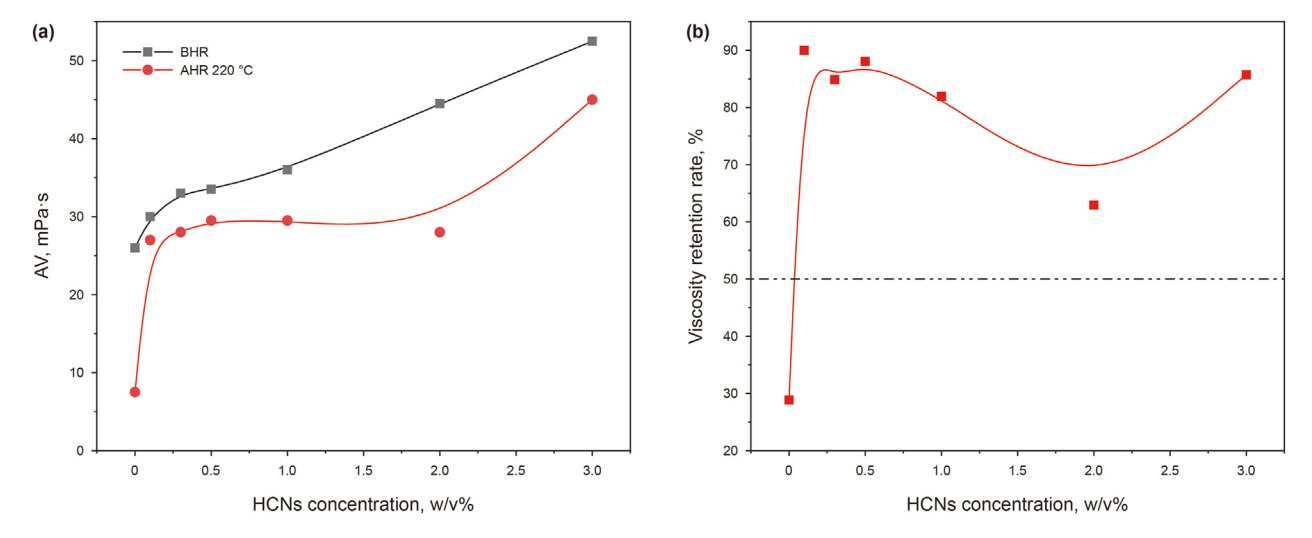


Fig. 11. (a) Variation of AV and (b) viscosity retention rate with HCNs content before and after dynamic aging at 220 °C.

XRD patterns of HCNs is presented in Fig. 5(d). A broad and low-intensity peak at 22.6° assigned to 002 reflection was observed, which means that HCNs are amorphous structures with low crystallinity, in agreement with the Raman spectrum result.

3.1.4. SEM and TEM

The morphology of HCNs was analyzed with SEM. Fig. 6(a) illustrates that many particles exhibited a spherical shape and smooth surfaces. A portion of these particles aggregated and fused,

resulting in structures resembling peanuts. Furthermore, measurements using Nano Measure 1.2 software indicated that the particle size distribution of HCNs spans from 150 to 460 nm, with an average particle size of 300 nm (Fig. 6(b)). The TEM images of HCNs are depicted in Fig. 6(c), which also corroborates the spherical morphology. Furthermore, previous morphological studies verified that hydrothermal carbons have core-shell structures that hydrophobic furan-rich polymer networks are in the core and various hydrophilic oxygenated functional groups are attached to the

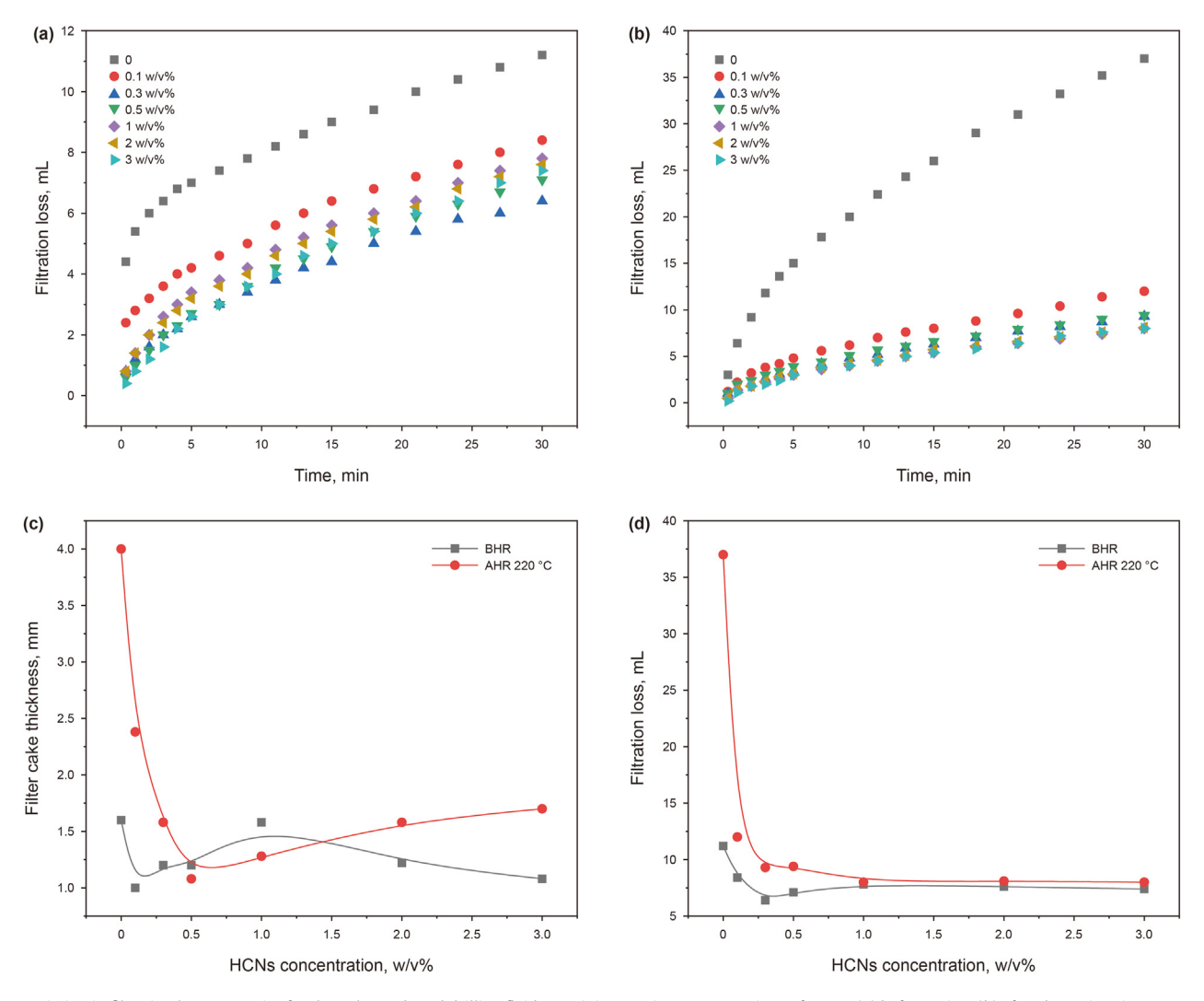


Fig. 12. Variation in filtration loss properties for the polymer-based drilling fluid containing varying concentrations of HCNs: (a) before aging, (b) after dynamic aging at 220 °C, (c) filter cake thickness prior to and after aging, (d) API filtration loss prior to and after aging.

surface (Higgins et al., 2020). Fig. 6(d) indicated that an amorphous and core-shell structure was also observed for HCNs, consistent with previous studies (Luo et al., 2024; Wang et al., 2017).

3.1.5. Particle size and zeta potential

As shown in Fig. 7, with the increase of pH value, the average particle size of HCNs aqueous dispersion exhibited a decreased trend while the absolute value of zeta potential increased gradually, which was ascribed from the increased deprotonation degree of oxygen-containing functional groups and enhanced repulsion between HCN particles at alkaline conditions (Tan et al., 2020). In addition, it could be seen that at weak alkaline conditions, which are also pH value range of typical water-based drilling fluids, HCNs can be well dispersed.

3.2. Rheological and filtration properties under high temperatures

3.2.1. Bentonite base mud with HCNs

Fig. 8(a) shows the plots of shear stress versus shear rate for bentonite base mud with various HCNs addition. When the HCNs concentration was between 0.1 w/v% and 0.5 w/v%, the values of shear stress were almost identical to that of bentonite base mud. A more significant increase of shear stress was noted when the HCNs

concentration reached 1.0 w/v%. Fig. 8(b) illustrates the changes in viscosity with shear rate as the increase of HCNs concentration. All the suspensions exhibited shear thinning non-Newtonian behavior. The viscosity decreased slightly as the addition of relatively low concentrations of HCNs. Similar to that of shear stress, when the HCNs concentration reach 1.0 w/v%. the viscosity was obviously higher than that of bentonite base mud. Due to the abundance of oxygen-containing functional groups, the initial addition HCNs raised the repulsion between the bentonite particles, which diminished the number of association structures and resulted in the reduction of viscosity. When the HCNs reached 1.0 w/v%, the high concentration of nanoparticles in turn increased the interaction between bentonite particles, corresponding to the increase of viscosity. The increased solid fraction and hydrogen bonding between HCNs and bentonite particles are probably responsible for this change (Kane et al., 2022). Various rheological models, including the Bingham, Power-law, and H-B models, were employed to fit the relationship between shear stress and shear rate. As shown in Table 2, the H-B model delivered the most accurate rheological fit, evidenced by the highest R^2 values. For HCNs with concentrations above 1.0 w/v%, the H-B model yielded higher *K* values and lower *n* values, suggesting an improved performance in carrying drilling cuttings.

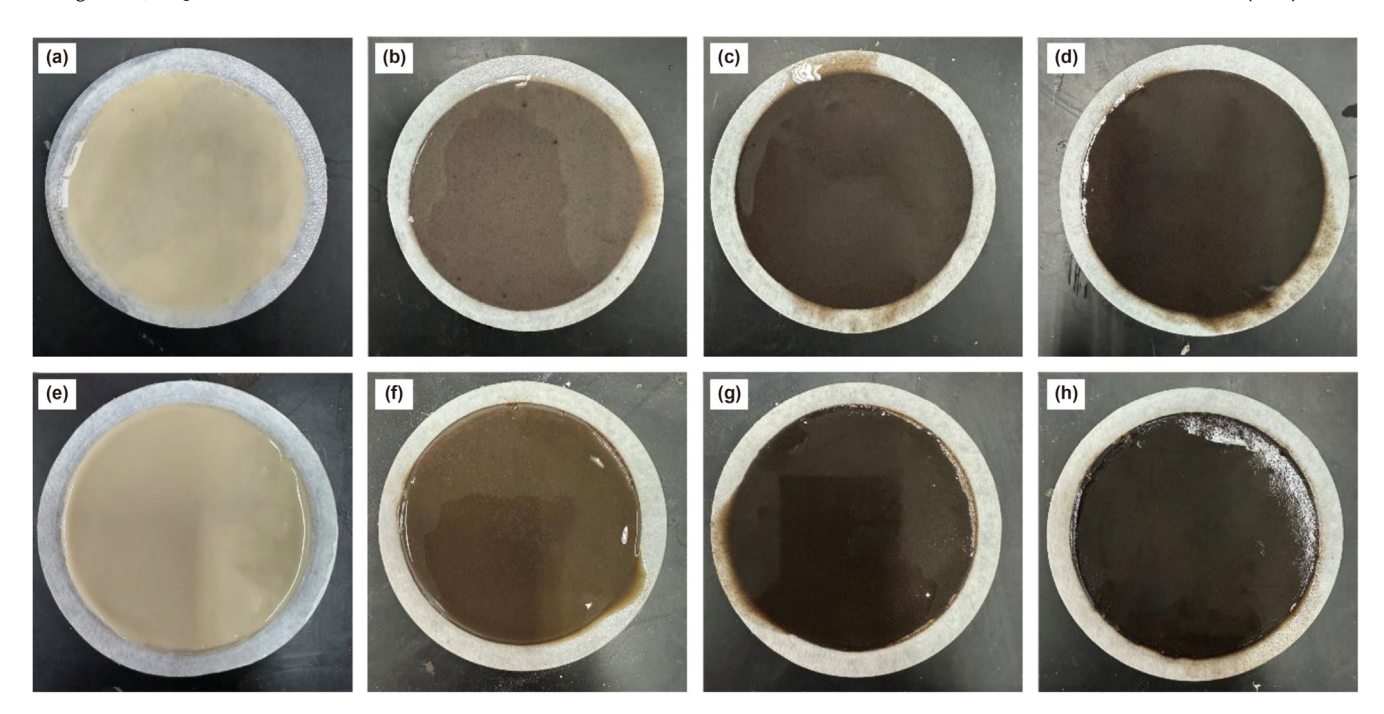


Fig. 13. API filtration loss cake photographs of different testing fluids: (**a**) control sample before hot rolling, (**b**) control sample with 0.3 w/v% HCNs before hot rolling, (**c**) control sample with 1.0 w/v% HCNs before hot rolling, (**d**) control sample with 3.0 w/v% HCNs before hot rolling, (**e**) control sample after hot rolling, (**f**) control sample with 0.3 w/v% HCNs after hot rolling, (**g**) control sample with 1.0 w/v% HCNs after hot rolling. (**h**) control sample with 3.0 w/v% HCNs after hot rolling.

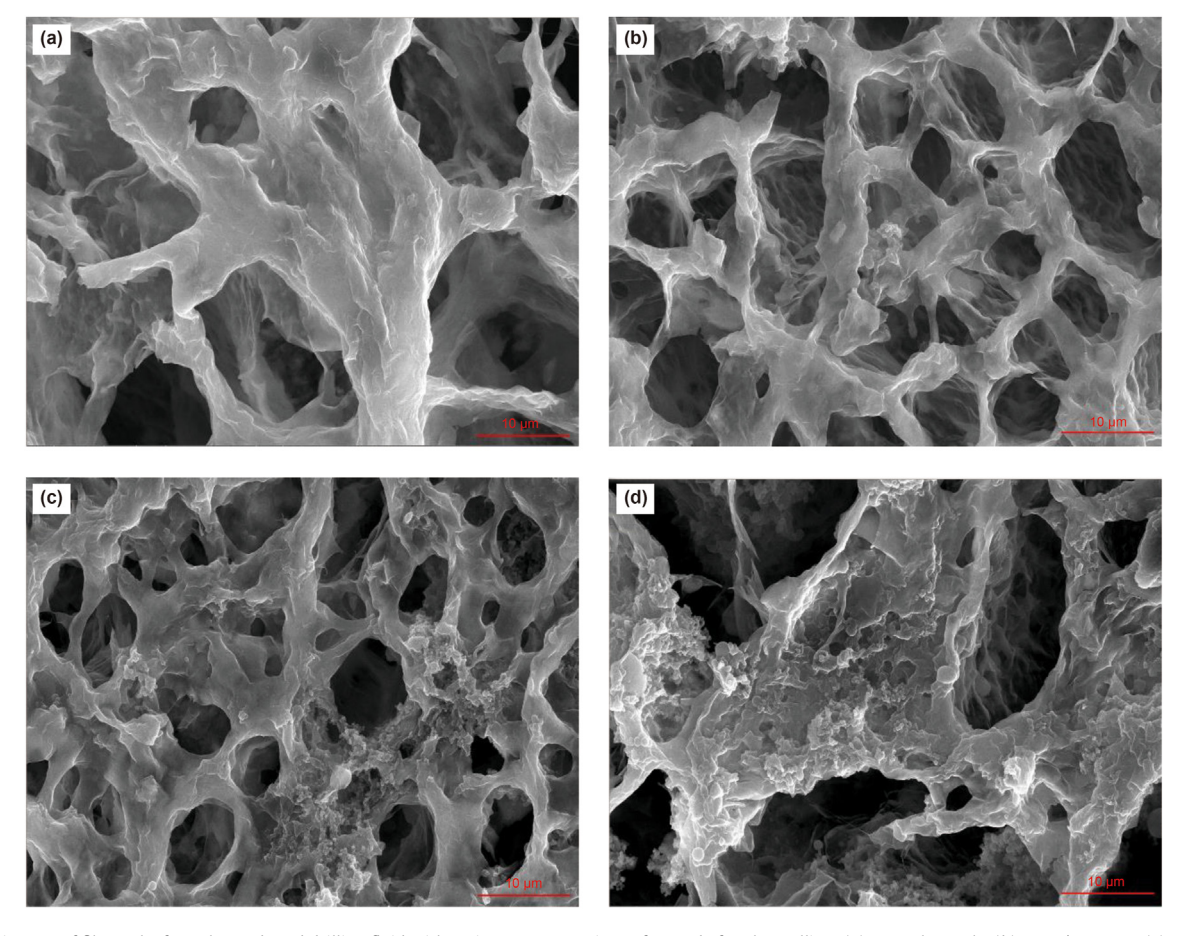


Fig. 14. SEM images of filter cake for polymer-based drilling fluid with various concentrations of HCNs before hot rolling: (a) control sample, (b) 0.3 w/v% HCNs, (c) 1.0 w/v% HCNs, (d) 3.0 w/v% HCNs.

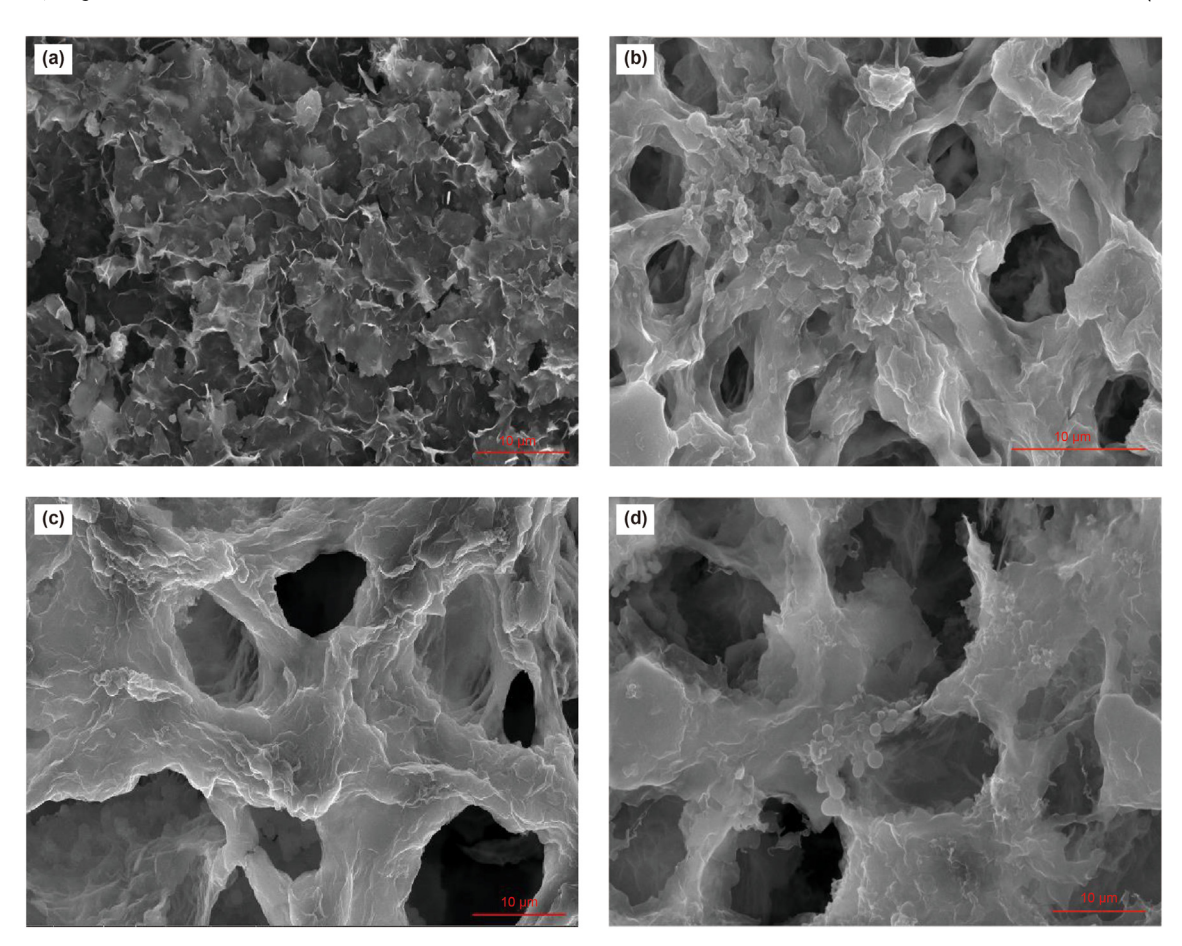


Fig. 15. SEM images of filter cake for polymer-based drilling fluid with various concentrations of HCNs after dynamic aging at 220 °C: (a) control sample, (b) 0.3 w/v% HCNs, (c) 1.0 w/v% HCNs, (d) 3.0 w/v% HCNs.

The bentonite-based mud, containing varying concentrations of HCNs, was dynamically aged at 220 °C for 16 h. Filtration tests were conducted both before and after dynamic aging. As shown in Fig. 9(a), before hot rolling, a minor increase in the filtration loss was observed when the HCNs concentration was lower than 0.5 w/ v%. Above that concentration the filtration loss exhibited a remarkable increase, which was probably attributed to the agglomeration of the excessive HCNs particles. As the bentonite suspension subjected to hot rolling, high temperature caused clay particles to dehydrate and aggregate into clusters. As a result, the filtration loss significantly increased from 13.6 to 41.8 mL. Due to the stable dispersion under elevated temperature conditions, the addition of HCNs into the bentonite suspension could effectively fill the micropores formed between aggregated clay particles, therefore resulted in the decrease of filtration loss. Specifically, a 50.7% reduction in filtration loss was achieved at 0.5 w/v% HCNs (Fig. 9(b)). At higher concentrations, the aggregation of HCNs particles may also occurred, which prevents the formation of effective sealing. Therefore, the filtration loss did not exhibit a monotonic decrease pattern but began to increase to some extent with further increase of HCNs concentration, though it remained significantly lower than that of the control sample, indicating that HCNs could efficiently reduce the filtration loss at appropriate concentrations after hot rolling.

3.2.2. Polymer-based drilling fluid with HCNs

3.2.2.1. Rheological properties. The rheological profiles of polymerbased drilling fluid with the increase of HCNs concentration is

presented in Fig. 10. As shown in Fig. 10(a), for HCNs between 0.1 w/ v% and 0.5 w/v%, the shear stress decreased with the increase of HCNs concentration at equal shear rates. For the HCNs above 1.0 w/ v%, the shear stress was higher than the control sample when the shear rate was higher than 200 s^{-1} . In the case of viscosity, as shown in Fig. 10(b), at low shear rate (less than 10 s^{-1}), the viscosity initially decreased and then began to increase at 1.0 w/v% HCNs, but still lower than control sample when the HCNs concentration reached 3.0 w/v%. At high shear rate (above 10 s^{-1}), the viscosity also decreased initially and then increased again, which was higher than control sample when the HCNs concentration reached 1.0 w/v%. Similar to that of bentonite base mud, the H-B model was also the best fitting model for the rheological curves. It was observed in Table 3 that the yield point (τ_0) generally decreased with the HCNs concentration, different from that of bentonite suspensions.

Fig. 11(a) shows the variation of rheological parameter AV for the polymer-based drilling fluid incorporated with varying concentrations of HCNs prior to and after dynamic aging at 220 °C. Howard (1995) indicated that a viscosity reduction rate of less than 50% after thermal aging at a specific temperature for 16 h is indicative of thermal stability. Thus, the percentage reduction in apparent viscosity (AV) can be used to assess the stability of the drilling fluid following hot rolling. As shown in Fig. 11(b), after dynamic aging, the degradation of polymer led to sharp loss of viscosity. The viscosity retention rate was less than 30%. While the addition of HCNs suppressed the viscosity decrease. It could be found that excellent viscosity retention rate was observed at low

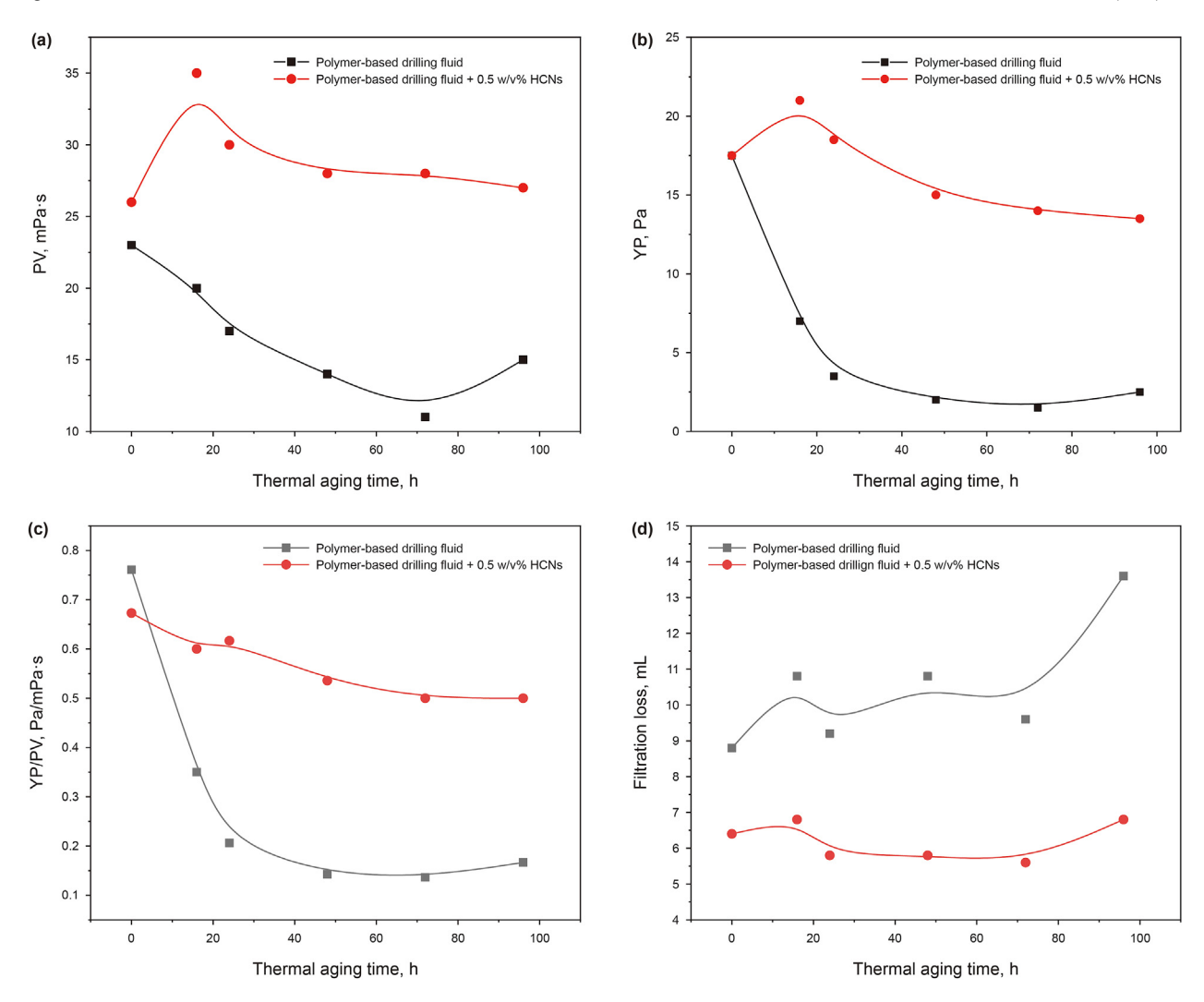


Fig. 16. Evolution of rheological parameters and API filtration loss with static thermal aging time for various testing fluids: (a) PV, (b) YP, (c) YP/PV, (d) Filtration loss.

Table 4 Variation of rheological and filtration loss for various bentonite-free water-based drilling fluid formulations before and after exposure to dynamic aging at $150\,^{\circ}$ C.

Formula	Fluid 1#		Fluid 2	#	Fluid 3	#	Fluid 4#	
Results	BHR	AHR	BHR	AHR	BHR	AHR	BHR	AHR
Φ600	63	13	61	45	45	29	49	51
Φ 300	45	8	48	31	29	16	31	32
Φ 200	37	5	39	24	21	11	24	24
Φ 100	27	3	28	16	14	6	11	11
Φ 6	8	0	6	2	3	1	3	3
Φ 3	6	0	5	1	2	0	2	2
pН	13.18	11.48	12.54	11.34	13.71	11.29	12.16	10.57
AV, mPa·s	31.5	6.5	30.5	22.5	22.5	14.5	24.5	25.5
PV, mPa·s	18	5	13	14	16	13	18	19
YP, Pa	13.5	1.5	17.5	8.5	6.5	1.5	6.5	6.5
ρ , g/cm ³	1.03	1.03	1.03	1.03	1.26	1.26	1.26	1.26
FL _{API} , mL	8	125.6	10.8	12.8	6.0	8.0	6.6	8.2

HCNs concentration (less than 0.5 w/v%). With the further increase of HCNs concentration, the viscosity maintained relatively stable after hot rolling at 220 °C. Clearly, the addition of low concentration of HCNs stabilized the rheology of polymer-based drilling fluid after exposure to such ultra-high temperatures.

3.2.2.2. Filtration properties. Fig. 12 illustrates the filtration

properties of polymer-based drilling fluid with HCNs before and after dynamic aging at 220 °C. Initially, the filtration rate for the polymer-based drilling fluid was high, but decreased after 5 min due to the formation of filter cake, as indicated by the change in the slope of the filtration curve (Fig. 12(a)). The presence of HCNs reduced the filtration rate and accelerated filter cake formation. This effect was more pronounced after hot rolling at 220 °C (Fig. 12(b)). Prior to thermal aging, the impact of HCNs on filtration properties was minimal, with only limited reductions in filter cake thickness and filtration loss. After hot rolling, due to polymeric additive degradation, filter cake thickness increased from 1.6 to 4 mm and filtration loss rose from 11.2 to 37 mL (Fig. 12(c) and (d)). However, these parameters significantly decreased with the addition of low concentrations of HCNs, and became stable with HCNs concentration above 0.5 w/v%. At 1.0 w/v% HCNs, the filtration loss was reduced by 78% compared to the base fluid. Fig. 13 shows that after dynamic aging, the filter cake of the control sample became thicker, while the filter cake with HCNs turned to be dark brown and smoother.

Figs. 14 and 15 present the SEM images of filter cakes for polymer-based drilling fluid with varying HCN contents, before and after dynamic aging at 220 °C respectively. Fig. 14(a) shows that for the polymer-based drilling fluid, the thorough hydration of bentonite particles and the adsorption of polymers created dense,

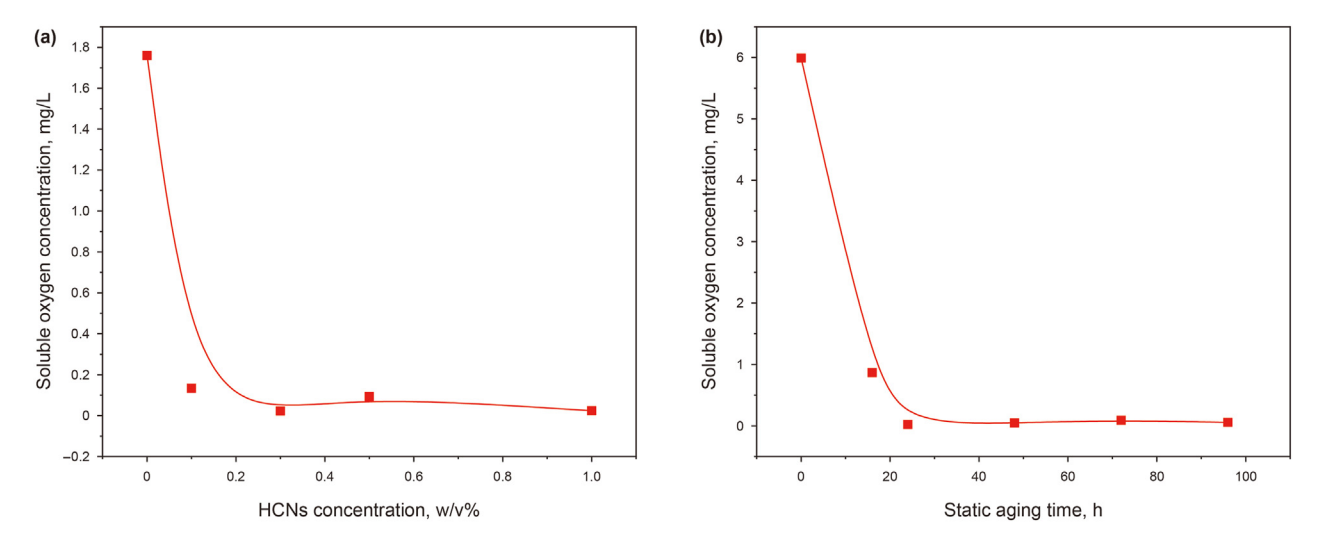


Fig. 17. Variation of soluble oxygen concentration for polymer-based drilling fluid under different conditions: (a) with varying concentrations of HCNs before and after hot rolling at 200 °C, (b) static thermal aging at 200 °C in the presence of 0.5 w/v% HCNs.

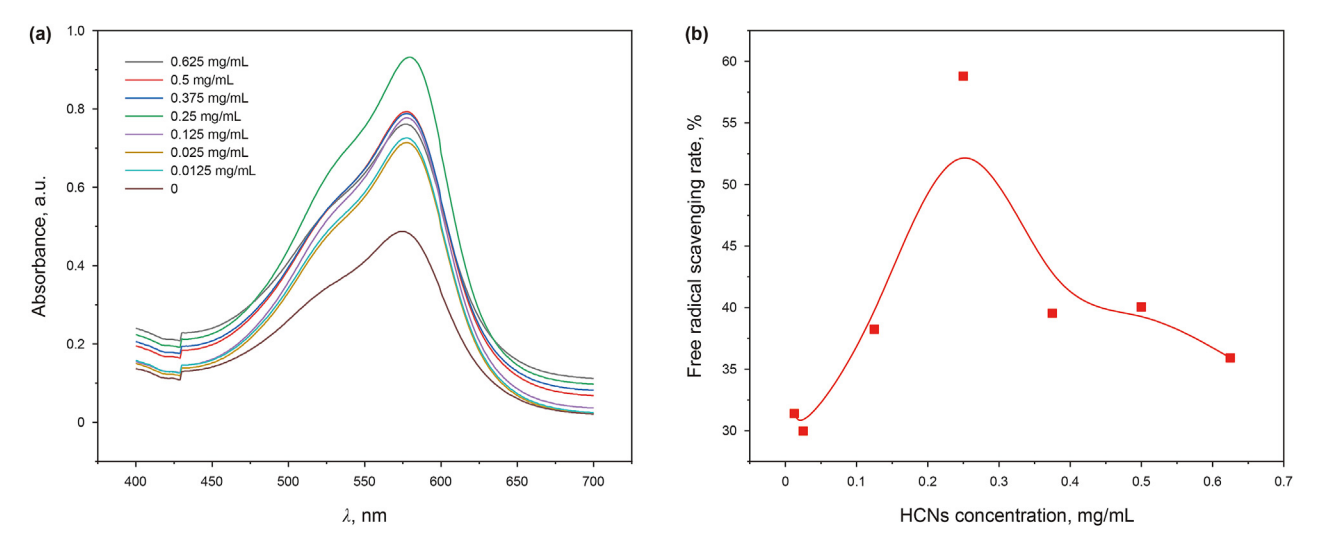


Fig. 18. Variation of (a) absorbance and (b)·OH free radical scavenging rate as a function of HCNs concentration.

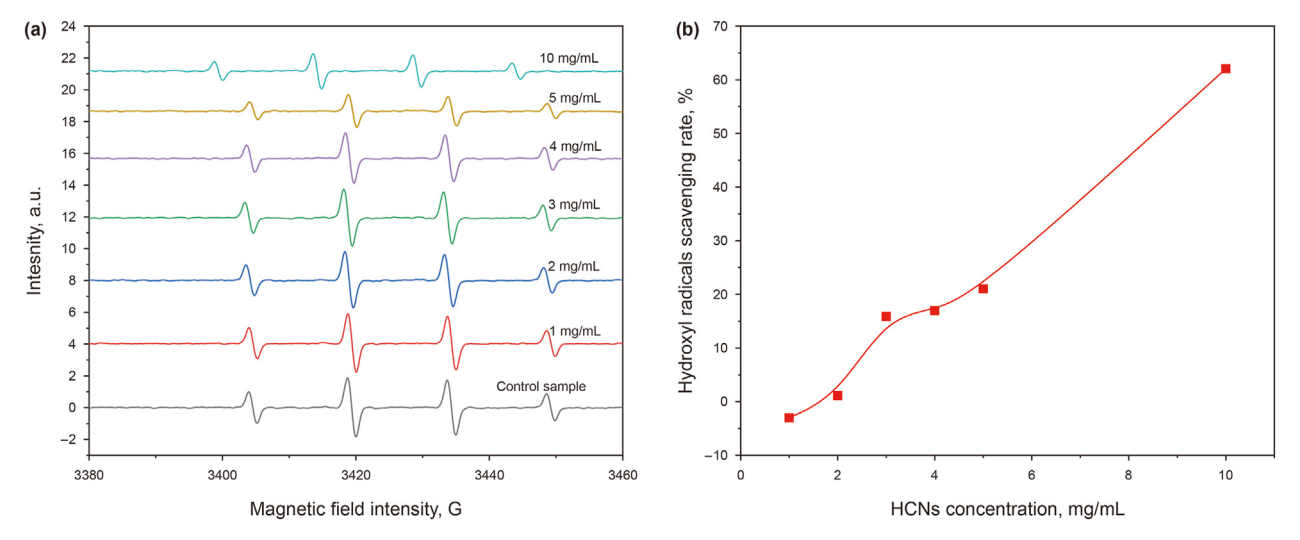


Fig. 19. The EPR spectra of DMPO-OH with different concentrations of HCNs: (a) EPR spectra, (b) hydroxyl radicals scavenging rate.

honeycomb-like network structures, resulting in a low-permeability filter cake and consequently low filtration loss. With the addition of HCNs, as depicted in Fig. 14(b-d), nanoparticle clusters obstructed the polymer networks, which further reduced the filtrate passage. This resulted in a decrease in filtration loss and the formation of thin, impermeable filter cakes.

When the polymer-based drilling fluid was thermally aged at 220 °C, as shown in Fig. 15(a), because of the degradation of polymers, the typical honeycomb-like network structures disappeared. Meanwhile, since the adsorbed water becomes more rigidly bonded to the clay at ~300 °F (Fisk and Jamison, 1989), aging at 220 °C remarkably alters the orientation of the adsorbed water on clay surface. The dispersion of clay particles decreases and a large amount of sheet-like aggregates form. Therefore, the filter cake becomes much more porous and allows a quite higher filtration loss value. After different concentrations of HCNs were added into the polymer-based drilling fluid (Fig. 15(b-d)), although the association of clay platelets occurred in a certain degree after thermal aging, severe flocculated and aggregated structures did not form. At the same time, the polymer networks still existed and numerous HCNs particles were also observed in the filter cake, which give low porosities and permeabilities of the filter cakes.

3.2.2.3. Long term thermal stability. In deep and ultra-deep well drilling, the trip time is much longer than that of shallow well. In the tripping operation, the circulation of drilling fluid stopped. The drilling fluids have to combat high temperature under downhole for a long time. Under such an extremely harsh condition, both

exposure temperature and heating duration should be considered during the thermal degradation process (Shin and Cho, 1998). To assess the impact of HCNs on the long-term thermal stability of polymer-based drilling fluid, the fluid was statically aged at 200 $^{\circ}\text{C}$ for various durations.

As shown in Fig. 16(a), the plastic viscosity (PV) of the polymer-based drilling fluid decreased progressively with the increase of aging time. Fig. 16(b) illustrates a dramatic drop in the yield point (YP) after 16 h of thermal aging. After aging at 24 h, the YP to PV ratio fell significantly and then fluctuated slightly, indicating reduced stability and poor drilling cuttings carrying capacity (Fig. 16(c)). In contrast, with 0.5 w/v% HCNs, both PV and YP remained considerably higher than those of the polymer-based drilling fluid at equivalent aging times. Additionally, PV and YP values changes relatively little with aging time, reflecting much greater thermal stability. The smaller reduction in rheological properties and lower filtration loss (Fig. 16(d)) with thermal aging further demonstrate the effectiveness of HCNs in enhancing the long-term stability of the polymer-based drilling fluid.

3.2.3. Bentonite-free water-based drilling fluid with HCNs

The variation of rheological and filtration properties for the bentonite-free water-based drilling fluid with and without HCNs before and after dynamic aging at 150 °C for 16 h is shown in Table 4. Because the used polymeric additives are mainly natural polymer derivatives, the bentonite-free water-based drilling fluid (Fluid 1#) exhibited a drastic decrease of rheological parameters after aging, and the filtration loss increased to as high as 125.6 mL.

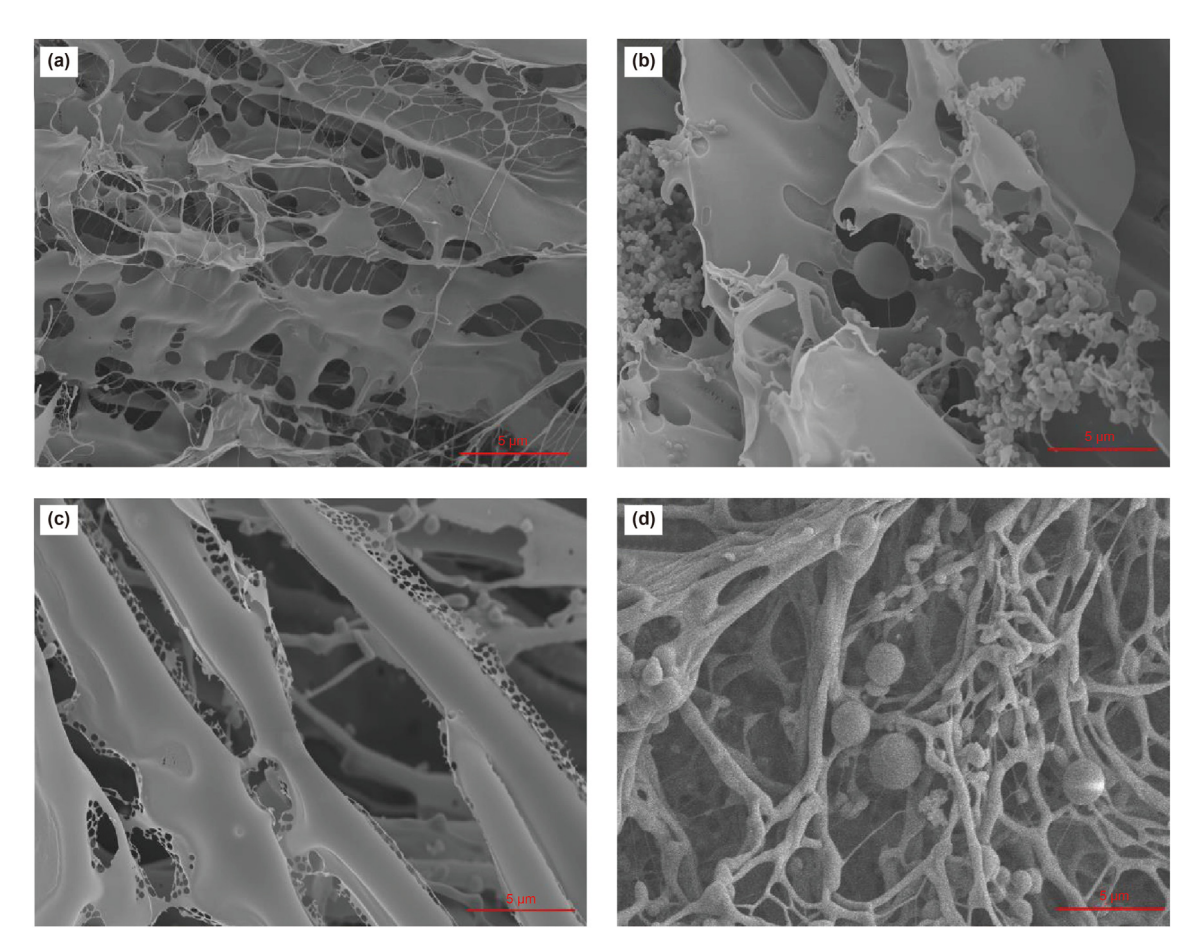


Fig. 20. Cryo-SEM images of HTSP solution with and without HCNs before and after hot rolling at 180 °C: (a) HTSP solution before hot rolling, (b) HTSP solution containing HCNs before hot rolling, (c) HTSP solution after hot rolling, (d) HTSP solution containing HCNs after hot rolling.

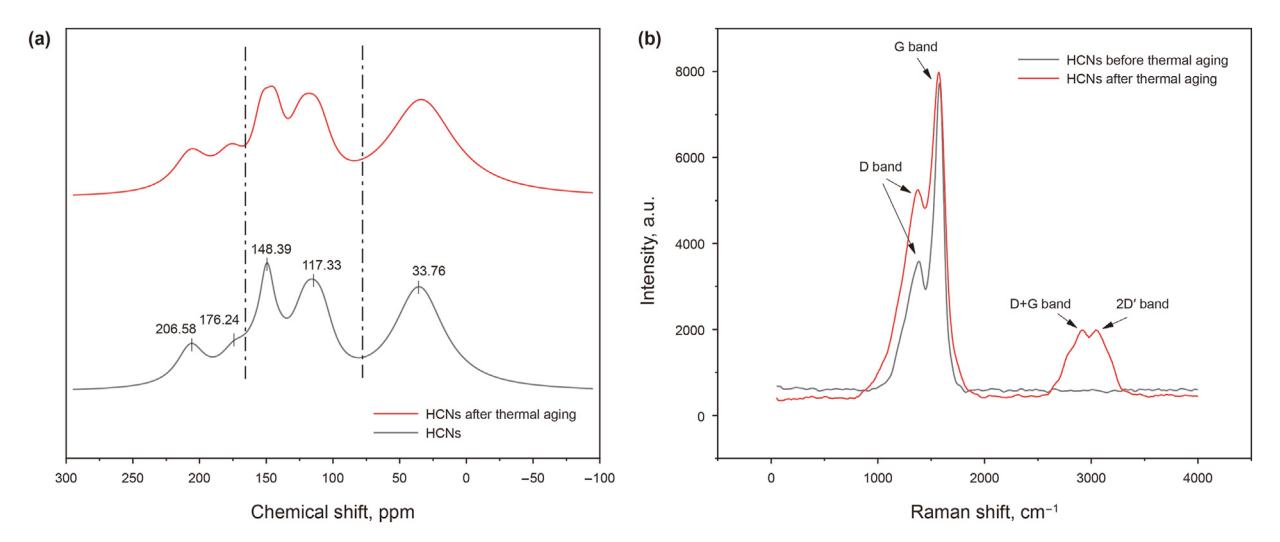


Fig. 21. (a) ¹³C solid-state NMR spectra and (b) Raman spectra of HCNs before and after thermal aging.

In the presence of 0.5 w/v% HCNs, a much better stable rheological parameters and lower filtration loss were observed for Fluid 2#, indicative of excellent thermal stability. When potassium formate was used for weighting material, a relative stable rheology and filtration properties were also observed after hot rolling due to the thermal stabilization effect of potassium formate (Fluid 3#). For xanthan gum, when the temperature reaches a critical point, the molecules change from a long rigid helical rod structure to a collapsed random coil, accompanied by the significant viscosity loss. The formate anions can improve the hydrogen bonding and self-association of water, therefore increase the transitional temperature of xanthan gum and delay the order-disorder conformational change (Howard and Downs, 2015). Meanwhile, formate potassium can act as a powerful reductant and anti-oxidant by scavenging the free radicals, which protects the polymers from thermal degradation (Bungert et al., 2000). These combined effects improved the thermal stability of the fluid at elevated temperatures. After incorporation of 0.5 w/v% HCNs, a further improvement in the stability of rheological properties after hot rolling was obtained (Fluid 4#), demonstrating a synergistic effect between potassium formate and HCNs.

3.2.4. High temperature stability mechanism

3.2.4.1. Soluble oxygen concentration measurement. During drilling operation, oxygen enters the drilling fluid at the surface, which is a key factor for the oxidative degradation of water-soluble polymers (Glass et al., 1983). The dissolved oxygen initiates oxidative degradation processes that lead to the breakage of molecular chains and removal of substituent groups, and corresponding drop in viscosity. When oxygen is present, the degradation rate of polymers mainly depends on the oxidation reaction (Gijsman, 2013). This phenomenon is often aggravated by the temperature. Previous study indicated that the viscosity of polymer decreases dramatically when only a small amount of dissolved oxygen is present (Yang et al., 2019). To avoid the polymer suffering severe degradation, it is necessary to minimize the concentration of dissolved oxygen as much as possible (Seright et al., 2010).

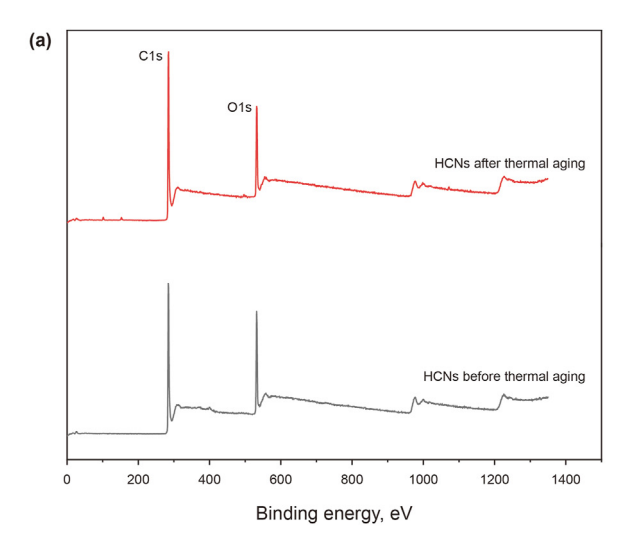
As shown in Fig. 17(a), for the polymer-based drilling fluid, because of the accelerated consumption of oxygen under high temperatures, the dissolved oxygen concentration decreased obviously with the increase of HCN concentration after hot rolling at 200 °C. The dissolved oxygen concentration of the fluids in the presence of HCNs was as low as approaching zero. In the process of

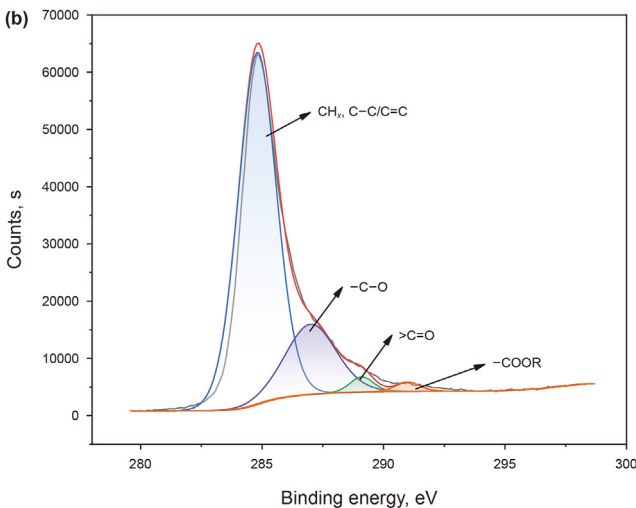
long-term thermal aging, as depicted in Fig. 17(b), the dissolved oxygen concentration for the polymer-based drilling fluid in the presence of 0.5 w/v% HCNs exhibited a rapid reduction and then maintained stable at near zero. These results indicated that HCNs can effectively exclude the oxygen from the drilling fluid and protect the polymers from oxygen attack.

3.2.4.2. Scavenging free radical. For biopolymers, they are easily attacked by one of the most reactive radicals, namely hydroxyl radical (Ash et al., 1983). As the strongest known oxidants, hydroxyl radicals can abstract hydrogen from the nearest organic molecules with no difference (Levitt and Pope, 2008). In this study, the hydroxyl radicals were generated by a classical Fenton reaction. The effect of HCNs on scavenging the hydroxyl radicals was probed by an indirect methyl violet UV-Vis spectroscopy method and a direct EPR method. As shown in Fig. 18(a), for the control sample, since the methyl violet was attacked by the highly reactive hydroxyl radicals, the solution became colorless and resulted in the low absorbance. As HCNs were incorporated, the absorbance gradually increased. As depicted in Fig. 18(b), the hydroxyl radical scavenging rate increased to 59% at 0.3 mg/mL HCNs, after that it decreased along with the increase of HCNs content.

The EPR spectra obtained from the samples of DMPO-OH with different concentration of HCNs are shown in Fig. 19(a). They are typically composed by a characteristic 1:2:2:1 quartet with hyperfine couplings (Han et al., 2011). The scavenging activity is evaluated by measuring the signal intensity of the second peak in solutions containing the HCNs with respect to a control without. The signal intensity decreased with the increase of HCNs concentration. As depicted in Fig. 19(b), when the concentration of HCNs reached 10 mg/mL, a 60% decline in free radical signal was observed, demonstrating an effective scavenging capability of HCNs for hydroxyl radicals. The difference between the results of methyl violet UV-Vis spectroscopy method and EPR method is still not clear, which needs further study.

3.2.4.3. Physical crosslinking interaction. Cryo-SEM is a powerful technique in characterizing microstructure of polymers. As shown in Fig. 20(a), for the synthetic polymers before thermal aging, numerous sheet-like and filamentous structures connected with each other were observed, which are responsible for the solution viscosity. In the presence of HCNs (Fig. 20(b)), a large number of spherical particles gathered together. Meanwhile, some particles





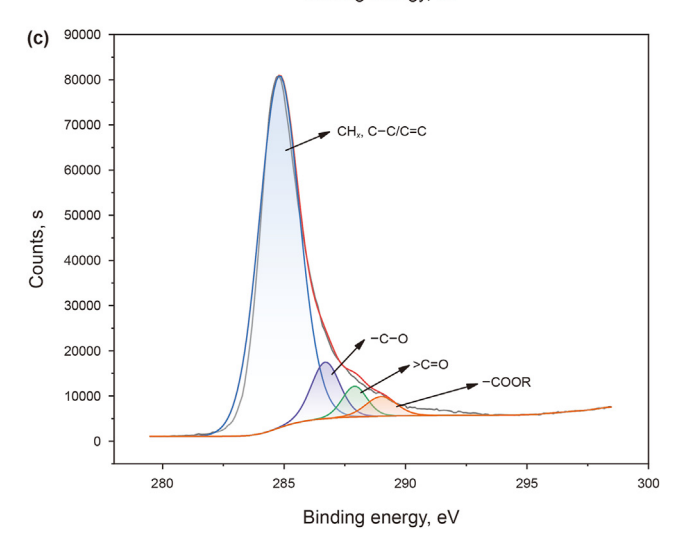


Fig. 22. (a) XPS fitted spectra of HCNs, C1s peaks of HCNs (b) before and (c) after thermal aging.

bridged between the polymers and formed networks, which act as physical crosslinkers between the polymer chains. After thermal aging at 180 °C, the appearance of the synthetic polymer changed. The wide sheet-like and filamentous structures disappeared (Fig. 20(c)). Relatively narrow strip structures with many

micropores on the edge were formed instead, which corresponded to the remarkable loss of viscosity and indicated the thermal degradation. However, for the solution with HCNs, as shown in Fig. 20(d), although the sheet-like structures of polymer disappeared and transformed into a rope-like structures, the favorable interaction between HCNs and polymer chains to cross-link and form networks is still visible, which demonstrated that the synthetic polymers are less susceptible to the thermal aging effect. HCNs played a vital role in reinforcing the thermal stability of synthetic polymers.

3.2.4.4. HCNs structure variation before and after thermal aging. As shown in Fig. 21(a), the ¹³C NMR spectra of HCNs can be categorized into three regions. Region I (0-80 ppm) represents sp³ carbon atoms. Region II (100–160 ppm) corresponds to sp² carbon atoms in C=C double bonds, with signals between 140 and 160 ppm specifically associated with oxygen-bound, O–C=C, sp² carbons. Region III (175-225 ppm) includes carbonyl groups such as carboxylic acids, ketones, and aldehydes (Titirici, 2013). After thermal aging at 200 °C, the peak areas at 148.39 and 117.33 ppm decreased from 21.08% to 12.23% and from 22.06% to 20.26%, respectively. Conversely, the peak area at 33.76 ppm increased from 42,23% to 51.33%. The reduction in peak area in Region II and the increase in Region I indicate a decrease in sp² carbon content in C=C double bonds and an increase in sp³ carbon content following thermal aging. This finding is further supported by the Raman spectra shown in Fig. 21(b). Before thermal aging, two distinct peaks of D band and G band were observed. After thermal aging, the ID/IG increased from 0.47 to 0.66, suggesting the decrease of sp² carbon atom content, which was probably attributed to the adduction reaction. In addition, two new peaks at 2930 and 3008 cm⁻¹ indicative of the D + G and 2D' band respectively appeared (Thapliyal et al., 2022), which also indicated the increased disorder degree of carbon materials.

The variation of chemical compositions of the HCNs before and after thermal aging was identified by XPS. Fig. 22(a) shows the C1s and O1s spectra of HCNs before and after thermal aging. The relative content of surface element C increased from 77.91% to 80.12%, and the relative content of O decreased from 22.09% to 19.88% after thermal aging. Fig. 22(b) and (c) present C1s spectrum of HCNs and their Lorentzian Gaussian peak fitting results before and after thermal aging treatment. The C1s spectra were deconvoluted into four peaks at 284.87, 286.98, 289.12 and 291.01 eV, which are attributed to aromatic ring carbon group (CH_x , C-C/C=C), hydroxide radical groups (-C-OR), carbonyl group (>C=O) and carboxyl groups, esters or lactones (-COOR), respectively (Zhang et al., 2023). Quantitative area analysis indicated that, after thermal aging, the relative area of the peak at 284.87, 289.12, and 291.01 eV increased from 76.45% to 82.57%, 1.99% to 4.43%, and 1.25% to 3.54%, respectively, while the relative area of the peak at 286.98 eV decreased from 20.31% to 9.46%. It was obvious that the relative content of surface -OH decreased while -COOR increased. During the thermal aging process, in the presence of a small amount of oxygen, the primary hydroxy groups would be oxidized into aldehyde groups and finally became carboxyl groups (Gao, 2012).

3.2.4.5. Mechanism analysis. During drilling operation, the drilling fluid is constantly in dynamic circulation, and oxygen in the air continuously dissolves into the drilling fluid. The contact with oxygen is unavoidable. The oxidation of polymeric additives is a radical chain reaction that may be initiated by the presence of oxygen. High temperature can accelerate this breakdown process dramatically. The thermal oxidative degradation results in the breakage of molecular chains and removal of substituent groups, which in turn leads to the rheology and filtration properties

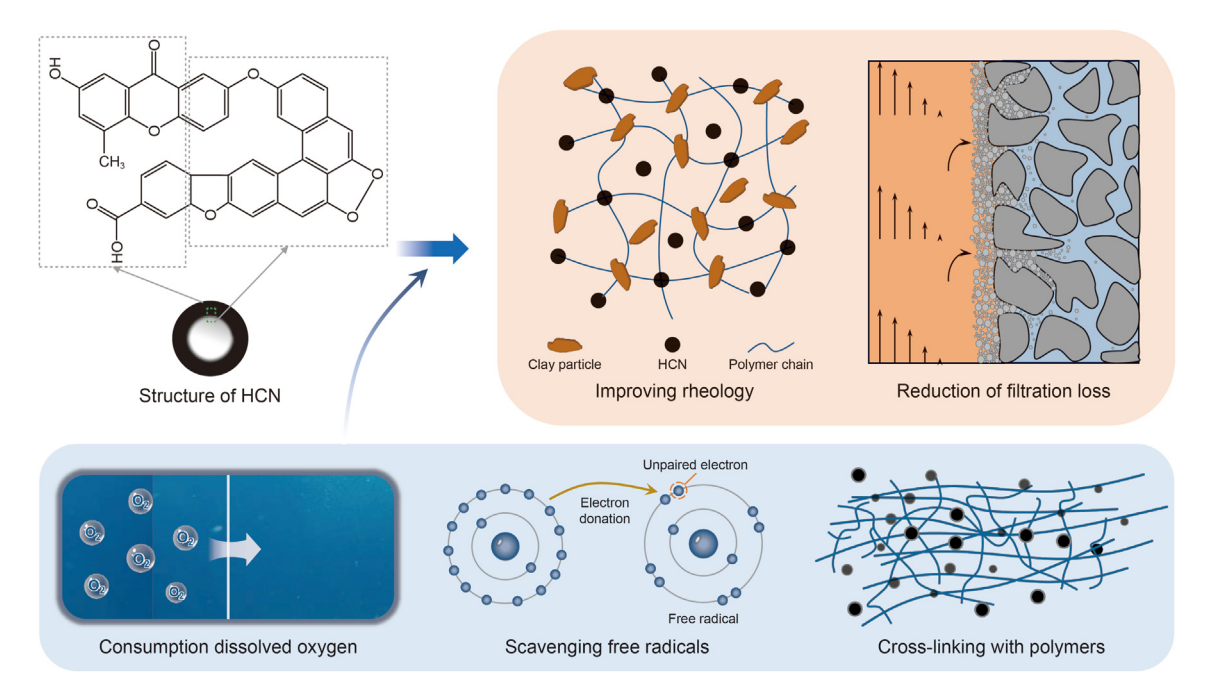


Fig. 23. Schematic diagram of enhancing the properties of water-based drilling fluid with respect to rheology and filtration using HCNs by a synergistic stabilizing mechanism.

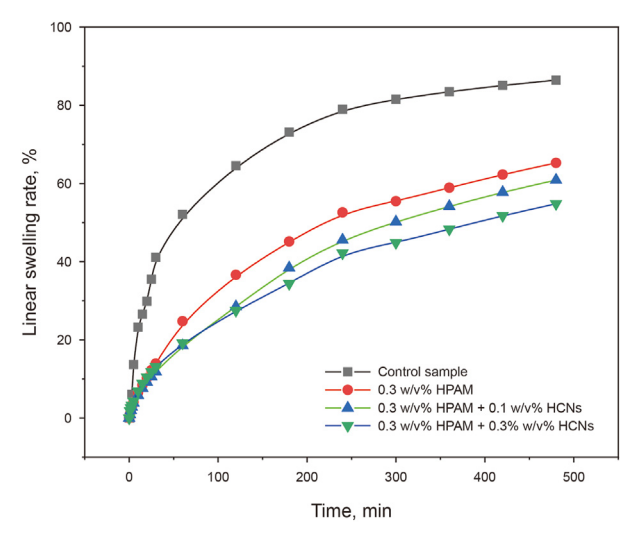


Fig. 24. Linear swelling rate of calcium bentonite pellet in various testing suspensions.

deterioration. Several approaches have been used to minimize oxidative degradation, such as removal of all dissolved oxygen and addition of free radical scavengers (Ferreira and Moreno, 2017).

HCNs are core-shell structures with abundant oxygen-containing surface functional groups and hydrophobic polyfuranic networks in the core (Luo et al., 2024). As stated above, HCNs preferably act as capturers of dissolved oxygen and therefore avoid the free radical formation and oxidative degradation. Meanwhile, based on the analysis of ultraviolet spectroscopy and EPR, due to the presence of surface hydroxyl groups and the sp² carbon core, HCNs can effectively scavenge the destructive hydroxyl radicals via hydrogen donation and radical adduction reaction (Li et al., 2023), which are involved in oxidative degradation processes at elevated temperatures, affording protection to polymers. Furthermore, the polymeric chains in the solution may be adsorbed on the HCNs surface via hydrogen bonds. HCNs can act as physical crosslinkers

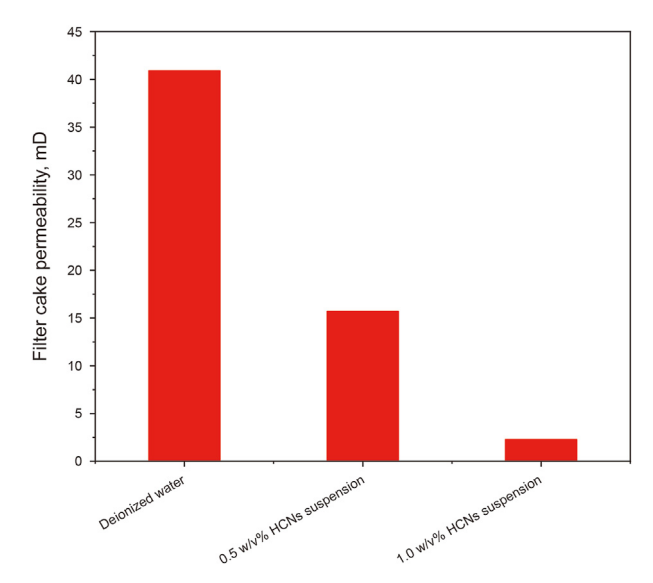


Fig. 25. Filter cake permeability after testing with various fluids.

between polymers, which makes the polymers difficult to be attacked by reactive radical species and less susceptible to the high temperatures. The above factors in combination contribute to the stability of polymers at elevated temperature conditions, which are premise to the rheology and filtration control. With respect to rheology and filtration properties, the networks formed between HCNs and polymers and the dispersed HCNs particles to plug the micropores of filter cake are also conducive for rheology stability and filtration loss control under harsh high temperatures (Fig. 23).

3.3. Shale stabilizing properties

3.3.1. Linear swelling test

When drilling into troublesome shale formations, the hydration and dispersion of shales induce complicated wellbore instability

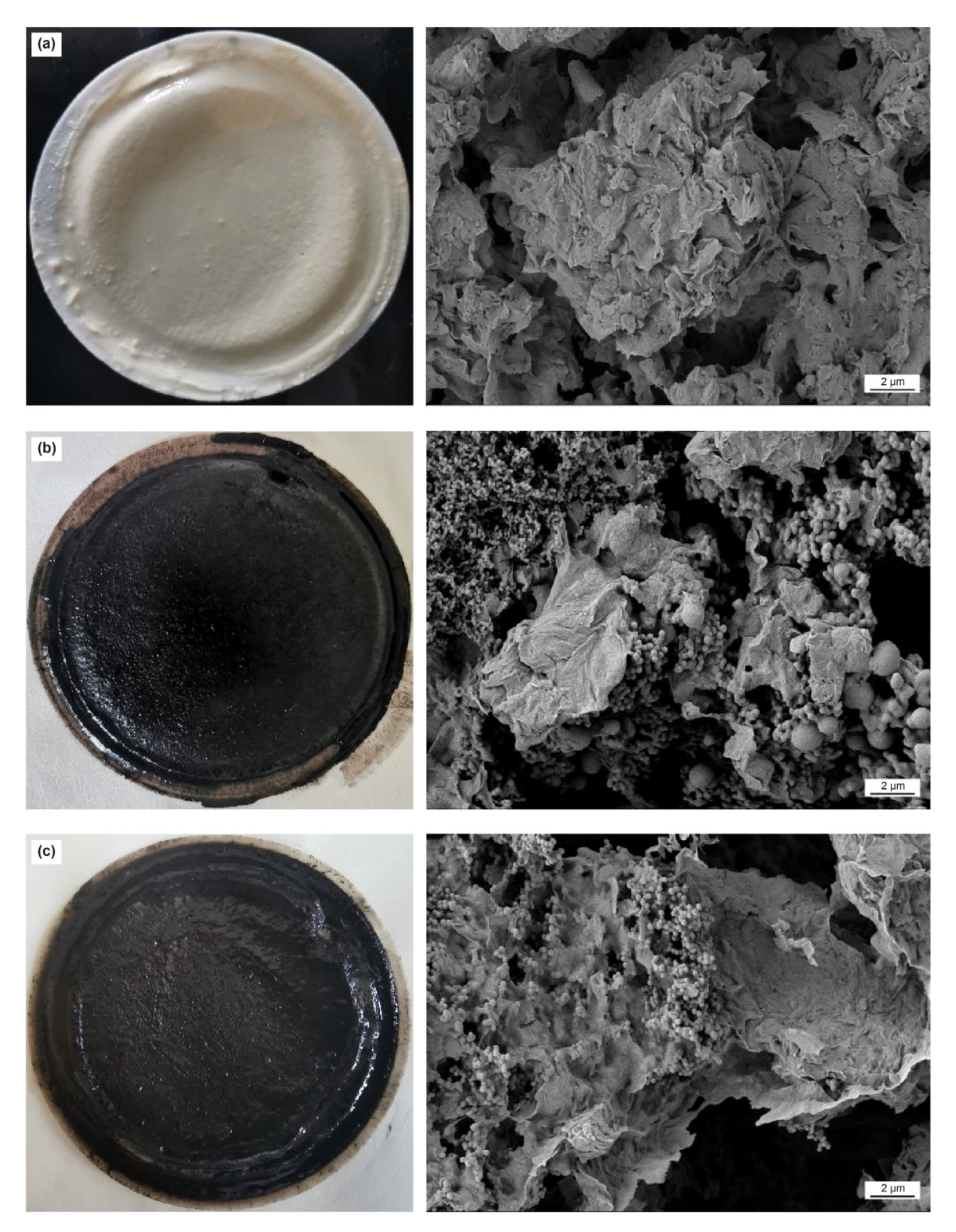


Fig. 26. Photographs (left) and SEM images (right) of filter cake obtained from calcium bentonite suspension with varying content of HCNs: (a) filter cake filtrated with deionized water, (b) filter cake filtrated with 0.5 w/v% HCNs suspension.

problems. The potential of HCNs in improving the shale stability was verified by linear swelling test and modified API filtration test. As shown in Fig. 24, for control sample, the calcium bentonite swelled quickly after contacting with deionized water. After testing for 180 min, the swelling rate approached an equilibrium. The swelling rate was 86.46% at the end of the test. The addition of HPAM slowed down the swelling rate, indicated that the adsorption

of HPAM onto clay surface impeded and retarded the penetration of water molecules. The swelling rate was reduced to 65.27%. Further incorporation of HCNs exhibited lower swelling rate, which further decreased to 54.82% at 0.3 w/v% HCNs, revealed that a synergistic effect between HCNs and HPAM. The physical sealing of HCNs probably contributed to this decreased water-clay interaction.

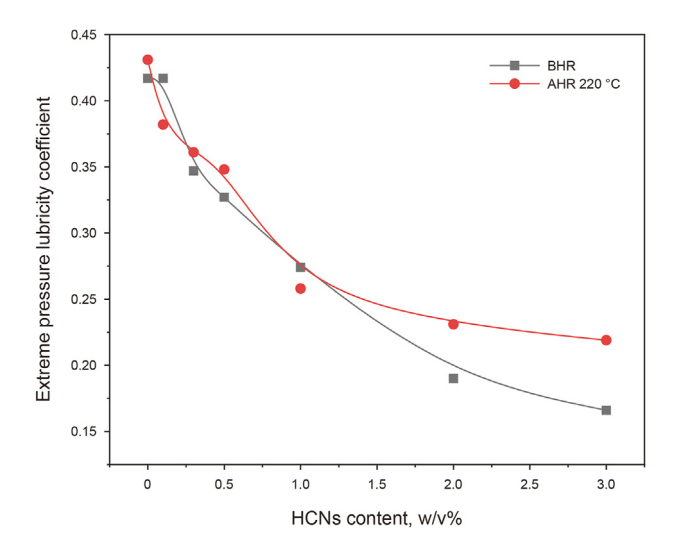


Fig. 27. The extreme pressure lubricity coefficient of polymer-based drilling fluid as a function of HCNs content before and after hot rolling at 220 $^{\circ}$ C.

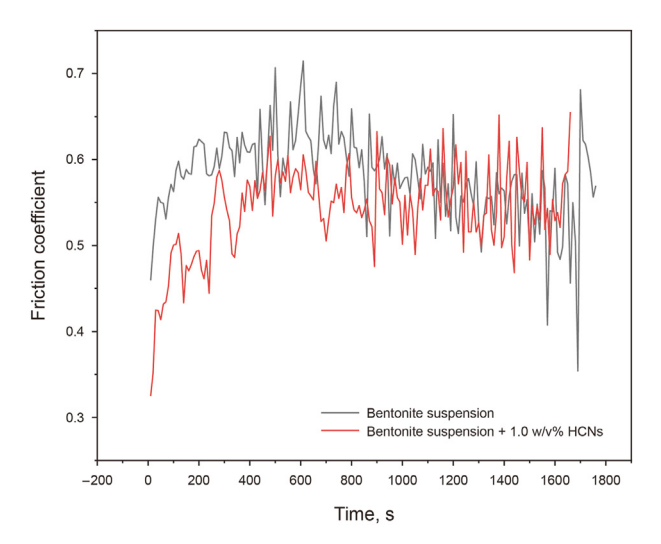


Fig. 28. Variation of friction coefficient of bentonite suspension with 1.0 w/v% HCNs as a function of time.

3.3.2. Modified filtration test

The physical sealing properties of HCNs were evaluated by a modified API filtration loss test. The decrease of permeability was used to indicate the water invasion minimization and the effectiveness of sealing the micropores of filter cake by HCNs. As shown in Fig. 25, using the calcium bentonite filter cake as the filtration medium, the permeability of the filter cake after seepage with deionized water, 0.5 w/v% HCNs suspension and 1.0 w/v% HCNs suspension was 40.9, 15.8, and 2.3 mD, respectively. It could be seen that addition of 1.0 w/v% HCNs into the suspension resulted in a 94.4% reduction of permeability, indicating extraordinary sealing performance. The SEM images of various filter cakes are present in Fig. 26. It was clear that for the control sample having calcium bentonite alone, a porous and loose filter cake was formed with aggregated calcium bentonite particles. After inclusion of HCNs, the adsorption of HCNs on the surface of clay particles plugged the micropores of the filter cake, which reduced the filtration channel of water molecules. As higher concentrations of HCNs were added, numerous tiny particles interacted with bentonite particles and formed a dense and impermeable filter cake, which caused the dramatic decrease of permeability. It could be inferred from the above tests that HCNs could inhibit clay hydration in combination with polymers and plug the micropores to prevent pressure transmission into the shales, which are essential for shale formation stability.

3.4. Lubrication performance

3.4.1. Extreme pressure lubricity test

The extreme pressure lubricity coefficient of polymer-based drilling fluid as a function of HCNs content before and after hot rolling at 220 °C is illustrated in Fig. 27. The lubricity coefficient decreased progressively with the increase of HCNs content. A reduction of 22% was obtained when 0.5 w/v% HCNs was added. Owing to the improvement of thermal stability by HCNs, the polymer-based drilling fluid maintained relatively stable after hot rolling at 220 °C where the lubricity coefficient showed a similar change trend as before thermal aging.

3.4.2. Four-ball friction test

The lubrication and anti-wear performance of HCNs were further evaluated by four-ball friction tests. As shown in Figs. 28 and 29, after addition of 1.0 w/v% HCNs into the bentonite suspension, the average friction coefficient was reduced from 0.5806 to 0.4656, accompanied with the average wear scar diameter decrease by 26%, implying HCNs could effectively reduce the friction. Numerous studies reported the lubrication mechanism of micro/nano spherical particles, which emphasized that the spherical particles could improve the tribological properties by converting sliding friction into rolling friction like ball bearings, forming a protective boundary film to prevent the direct contact of wear surfaces, filling the gap of friction surface and repairing the wear scars, and acting as polishing agents to reduce the roughness of friction surfaces (He et al., 2022; Lyu et al., 2021; Wu et al., 2019). HCNs may decrease the friction by one or a combination of the above mechanisms.

4. Conclusions

In this study, hydrothermal carbon nanospheres (HCNs) were synthesized using glucose as a precursor through a green hydrothermal carbonization process and introduced to improve the properties of water-based drilling fluids for the first time. The following conclusions can be deduced from the study:

- (1) HCNs had minimal impact on the rheological behavior of bentonite base mud but significantly reduced its filtration loss after thermal aging at 220 °C. A 50.7% reduction was observed at 0.5 w/v% HCNs. For polymer-based drilling fluid, HCNs also had a minor effect on rheology. The H-B model was the best fit for the rheological curves before thermal aging. After hot rolling at 220 °C, viscosity retention increased from 29% to 63%-90% with varying HCN concentrations, and filtration loss decreased by 78% with 1.0 w/v% HCNs. The polymer-based drilling fluid with 0.5 w/v% HCNs maintained stable rheology and low filtration loss after static thermal aging at 200 °C for 96 h. For a bentonite-free waterbased drilling fluid primarily made with modified natural polymers, the viscosity retention increased from 21% to 74% after hot rolling at 150 °C in the presence of 0.5 w/v% HCNs, and further increased when HCNs and potassium formate were employed in combination.
- (2) Owing to abundant oxygen-containing functional groups and sp² C=C bonds, HCNs could effectively trap dissolved oxygen and scavenge free radicals, preventing thermal oxidative

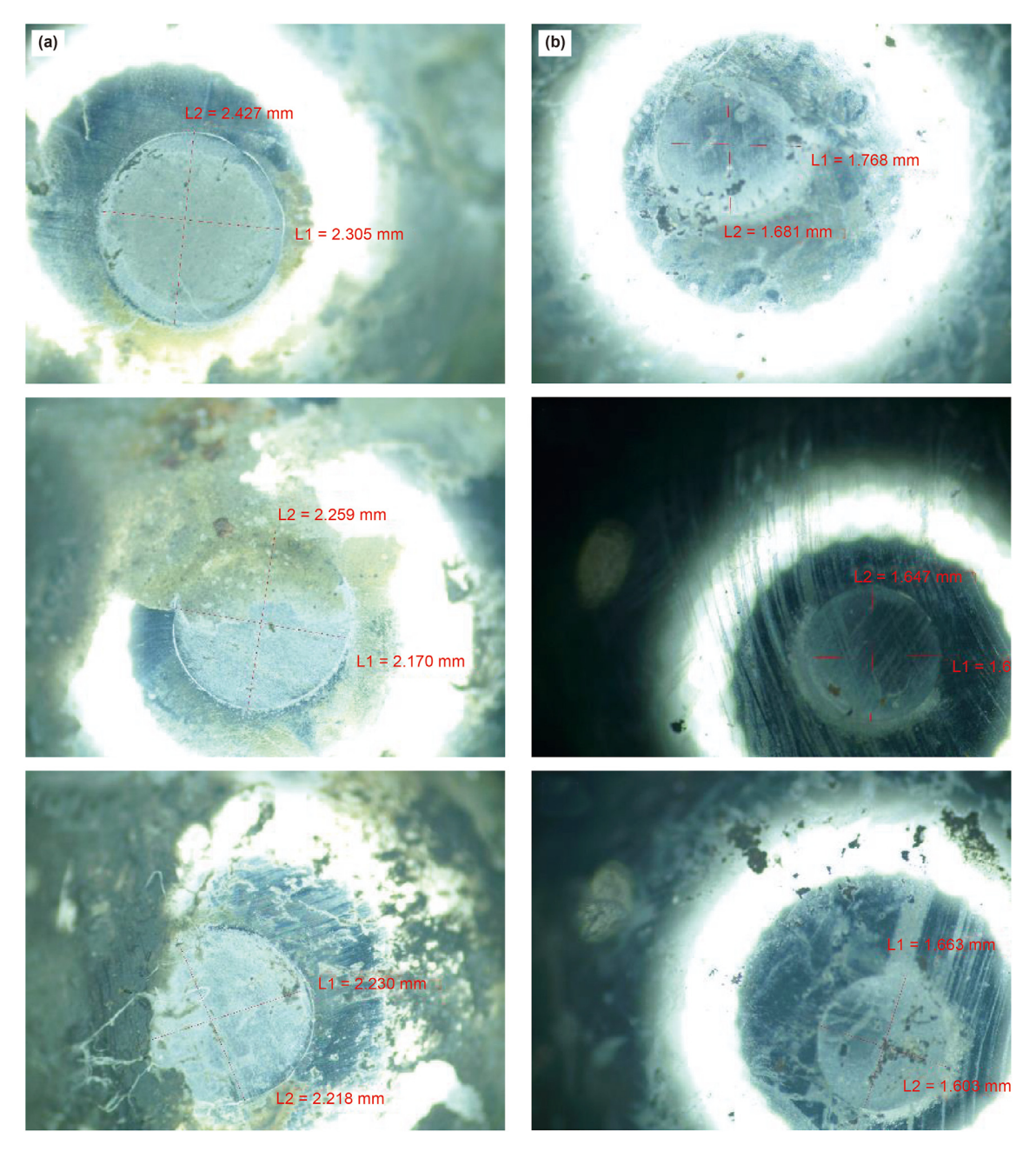


Fig. 29. Surface morphology of the lower ball wear area in the four-ball friction experiment: (a) bentonite base mud, (b) bentonite base mud with 1.0 w/v% HCNs. Up: No. 1 ball; Middle: No. 2 ball; Down: No. 3 ball.

degradation of polymers. Additionally, cross-linking interactions between HCNs and polymers contributed to thermal stability. The high-temperature stabilization effect and nano-size of HCNs significantly enhanced the rheological and filtration properties of water-based drilling fluid at elevated temperatures.

- (3) HCNs could inhibit clay hydration and swelling in synergy with partially hydrolyzed polyacrylamide and physically seal the micropores, contributing to shale formation stability.
- (4) HCNs could reduce the extreme pressure lubricity coefficient of polymer-based drilling fluid by 49% after thermal aging at 220 °C. The four-ball friction test implied that HCNs effectively improved the lubrication and anti-wear performance of bentonite base mud.
- (5) The environmental-friendly and sustainable HCNs played a multifunctional role in extending thermal stability, improving rheology and filtration loss, enhancing wellbore stability of shale formations and raising the lubrication properties of water-based drilling fluid. This study also paves the way for novel applications of hydrothermal carbon materials.

CRediT authorship contribution statement

Han-Yi Zhong: Writing — review & editing, Writing — original draft, Methodology, Investigation, Data curation, Conceptualization. **Shu-Sen Li:** Methodology, Investigation, Data curation. **Da-Qi**

Li: Project administration, Funding acquisition, Data curation. **Jun-Bin Jin:** Funding acquisition, Conceptualization. **Chang-Zhi Chen:** Methodology. **Zheng-Song Qiu:** Supervision, Investigation. **Wei-An Huang:** Project administration, Methodology.

Declaration of competing interest

The authors declare that they have no known competing financial interests or personal relationships that could have appeared to influence the work reported in this paper.

Acknowledgements

This work was financially supported by National Natural Science Foundation of China (No. 52174013), the Fundamental Research Funds for the Central Universities (24CX02004A), Natural Science Foundation of Shandong Province (ZR2024ME105), The Open Fund for Sinopec's Key Laboratory of Ultra-Deep Well Drilling Engineering and Technology (36650000-23-ZC0607-0063), and the Fund of State Key Laboratory of Deep Oil and Gas, China University of Petroleum (East China).

References

- Abu-Jdayil, B., 2011. Rheology of sodium and calcium bentonite-water dispersions: effect of electrolytes and aging time. Int. J. Miner. Process. 98 (3–4), 208–213. https://doi.org/10.1016/j.minpro.2011.01.001.
- Affede, L., Giubertoni, M., Ciuca, A., et al., 2023. Extreme efficiency from high performance water-based mud under HPHT conditions. ADIPEC. Abu Dhabi, UAE. https://doi.org/10.2118/216620-MS.
- Aftab, A., Ismail, A.R., Ibupoto, Z.H., et al., 2017. Nanoparticles based drilling muds a solution to drill elevated temperature wells: a review. Renew. Sustain. Energy Rev. 76, 1301–1313. https://doi.org/10.1016/j.rser.2017.03.050.
- Akaighe, N., Zeilinger, S., Cutler, J., et al., 2023. Low friction drilling fluid additive technology. SPE/IADC International Drilling Conference and Exhibition, Stavanger, Norway. https://doi.org/10.2118/212480-MS.
- Ash, S.G., Clarke-Sturman, A.J., Calvert, R., et al., 1983. Chemical stability of biopolymer solutions. The 58th Annual Technical Conference and Exhibition. San Francisco, California, USA. https://doi.org/10.2118/12085-MS
- Aydincak, K., Yumak, T., Sinağ, A., et al., 2012. Synthesis and characterization of carbonaceous materials from saccharides (glucose and lactose) and two waste biomasses by hydrothermal carbonization. Ind. Eng. Chem. Res. 51, 9145–9152. https://doi.org/10.1021/je301236h.
- Beg, M., Kesarwani, H., Sharma, S., 2019. Effect of CuO and ZnO nanoparticles on efficacy of poly 4-styrene sulfonic acid-co-maleic acid sodium salt for controlling HPHT filtration. Abu Dhabi International Petroleum Exhibition & Conference. Abu Dhabi, UAE. https://doi.org/10.2118/197703-MS
- Bungert, D., Maikranz, S., Sundermann, R., et al., 2000. The Evolution and Application of Formate Brines in High-Temperature/high-Pressure Operations. IADC/SPE Drilling Conference. New Orleans, Louisiana, USA. https://doi.org/10.2118/59191-MS.
- Chen, W., Wang, R., Zhang, Y., et al., 2023. HPLC, fluorescence spectroscopy, UV spectroscopy and DFT calculations on the mechanism of scavenging ·OH radicals by hypericin. J. Mol. Struct. 1274, 134472. https://doi.org/10.1016/i.molstruc.2022.134472.
- Ezell, R.G., Ezzat, A.M., Turner, J.K., et al., 2010. New filtration-control polymer for improved brine-based reservoir drilling-fluids performance at temperatures in excess of 400 °F and high pressure. SPE International Symposium and Exhibition on Formation Damage Control. Lafayette, Louisiana, USA. https://doi.org/10. 2118/128119-MS.
- Fang, Y., Liu, L., Xiang, H., et al., 2022. Biomass-based carbon microspheres for removing heavy metals from the environment: a review. Mater. Today Sustain. 18, 100136. https://doi.org/10.1016/j.mtsust.2022.100136.
- Ferreira, V.H.S., Moreno, R.B.Z.L., 2017. Polyacrylamide mechanical degradation and stability in the presence of iron. Offshore Technology Conference Brasil. Rio de Janeiro, Brazil. https://doi.org/10.4043/27953-MS.
- Fisk, J.V., Jamison, D.E., 1989. Physical properties of drilling fluids at high temperatures and pressures. SPE Drill. Complet. 4 (4), 341–346. https://doi.org/ 10.2118/17200-PA.
- Gao, X.Y., 2012. Preparation and Electrochemical Performance of Cellulose-Carbon Microspheres via Hydrothermal Carbonization. Master's Thesis. Taiyuan University of Technology (in Chinese).
- Gijsman, P., 2013. Review on the thermo-oxidative degradation of polymers during processing and in service. E-Polymers 8 (1), 1–34. https://doi.org/10.1515/epoly.2008.8.1.727.
- Glass, J.E., Soules, D.A., Ahmed, H., 1983. Viscosity Stability of Aqueous Polysaccharide Solutions. SPE California Regional Meeting, Ventura, California, USA.

https://doi.org/10.2118/11691-MS.

- Halali, M.A., Ghotbi, C., Tahmasbi, K., et al., 2016. The role of carbon nanotubes in improving thermal stability of polymeric fluids: experimental and modeling. Ind. Eng. Chem. Res. 55 (27), 7514–7534. https://doi.org/10.1021/ acs.ject.6b00784.
- Han, S.K., Hwang, T.M., Yoon, Y., et al., 2011. Evidence of singlet oxygen and hydroxyl radical formation in aqueous goethite suspension using spin-trapping electron paramagnetic resonance (EPR). Chemosphere 84 (8), 1095–1101. https:// doi.org/10.1016/i.chemosphere.2011.04.051.
- Hassiba, K.J., Amani, M., 2012. Salinity effect on the rheological properties of water based mud under high pressures and high temperatures of deep wells. SPE Kuwait International Petroleum Conference and Exhibition. Kuwait City, Kuwait. https://doi.org/10.2118/163315-MS
- He, T., Chen, N., Fang, J., et al., 2022. Micro/nano carbon spheres as liquid lubricant additive: achievements and prospects. J. Mol. Liq. 357, 119090. https://doi.org/ 10.1016/j.molliq.2022.119090.
- Higgins, L.J.R., Brown, A.P., Harrington, J.P., et al., 2020. Evidence for a core-shell structure of hydrothermal carbon. Carbon 161, 423–431. https://doi.org/ 10.1016/j.carbon.2020.01.060.
- Howard, S., Downs, J., 2015. Xanthan stability in formate brines- formulating nondamaging fluids for high temperature applications. SPE European Formation Damage Conference and Exhibition. Budapest, Hungary. https://doi.org/10.2118/ 174228-MS
- Howard, S.K., 1995. Formate brines for drilling and completion: state of the art. SPE Annual Technical Conference & Exhibition, Dallas, USA. https://doi.org/10.2118/30498-MS
- Inada, M., Enomoto, N., Hojo, J., et al., 2017. Structural analysis and capacitive properties of carbon spheres prepared by hydrothermal carbonization. Adv. Powder Technol. 28 (3), 884–889. https://doi.org/10.1016/j.apt.2016.12.014.
- Ischia, G., Cutillo, M., Guella, G., et al., 2022. Hydrothermal carbonization of glucose: secondary char properties, reaction pathways, and kinetics. Chem. Eng. J. 449, 137827. https://doi.org/10.1016/j.cej.2022.137827.
- Jaruwat, D., Udomsap, P., Chollacoop, N., et al., 2018. Effects of hydrothermal temperature and time of hydrochar from cattail leaves. AIP Conf. Proc. 2010 (1), 020016. https://doi.org/10.1063/1.5053192.
- Kamal, M.S., Ahmad, H.M., Murtaza, M., et al., 2023. Smart drilling fluids formulations for sensitive shale formations using surfactants and nanoparticles. SPE Western Regional Meeting. Anchorage, Alaska, USA. https://doi.org/10.2118/212966-MS
- Kane, A., Yang, J., Velmurugan, N., et al., 2022. Novel environmentally friendly nanoadditives for drilling fluid. Paper Presented at the 56th US Rock Mechanics/ Geomechanics Symposium, Santa Fe, New Mexico, USA. https://doi.org/ 10.56952/ARMA-2022-0719.
- Lankone, R.S., Deline, A.R., Barclay, M., et al., 2020. UV-Vis quantification of hydroxyl radical concentration and dose using principal component analysis. Talanta 218, 121148. https://doi.org/10.1016/j.talanta.2020.121148.
- Levitt, D.B., Pope, G.A., 2008. Selection and screening of polymers for enhanced -oil recovery. SPE/DOE Improved Oil Recovery Symposium. Tulsa, Oklahoma, USA. https://doi.org/10.2118/113845-MS
- Li, Q., Shen, X., Xing, D., 2023. Carbon quantum dots as Ros-generator and scavenger: a comprehensive review. Dyes Pigments 208, 110784. https://doi.org/10.1016/j.dyepig.2022.110784.
- Luo, Y., Lu, T., Jin, S., et al., 2024. Elucidating the intrinsic core-shell structure of carbon nanospheres from glucose hydrothermal carbonization. J. Supercrit. Fluids 210, 106290. https://doi.org/10.1016/j.supflu.2024.106290.
- Lyu, C., Hao, S., Yang, L., 2021. Application of nanosilica in glycerol-based drilling fluid for shale formations. SPE Drill. Complet. 36 (3), 473–482. https://doi.org/ 10.2118/204238-PA
- Mittag, J., Trutschel, L., Kruschwit, H., et al., 2022. Characterization of radicals in polysorbate 80 using electron paramagnetic resonance (EPR) spectroscopy and spin trapping. Int. J. Pharm. (Amst.) 4, 100123. https://doi.org/10.1016/ j.ijpx.2022.100123.
- Murtaza, M., Rana, A., Ahmad, H.M., et al., 2023. Performance evaluation of iron oxide and graphite nanoparticles in water-based drilling muds at HPHT conditions. Middle East Oil, Gas and Geosciences Show, Manama, Bahrain. https://doi.org/10.2118/213963-MS
- Rafati, R., Smith, S.R., Hadda, A.S., et al., 2018. Effect of nanoparticles on the modifications of drilling fluids properties: a review of recent advances. J. Petrol. Sci. Eng. 161, 61–76. https://doi.org/10.1016/j.petrol.2017.11.067.
- Rana, A., Khan, I., Saleh, T.A., 2021. Advances in carbon nanostructures and nanocellulose as additives for efficient drilling fluids: trends and future perspective-A review. Energy Fuel. 35 (9), 7319–7339. https://doi.org/10.1021/ acs.energyfuels.0c04341.
- Saha, N., Saba, A., Reza, M.T., 2019. Effect of hydrothermal carbonization temperature on pH, dissociation constants, and acidic functional groups on hydrochar from cellulose and wood. J. Anal. Appl. Pyrolysis 137, 138–145. https://doi.org/10.1016/j.jaap.2018.11.018.
- Sensoy, T., Chenevert, M.E., Sharma, M.M., 2009. Minimizing water invasion in shale using nanoparticles. SPE Annual Technical Conference and Exhibition. New Orleans, Louisiana, USA. https://doi.org/10.2118/124429-MS.
- Seright, R.S., Campbell, A.R., Mozley, P.S., et al., 2010. Stability of partially hydrolyzed polyacrylamides at elevated temperatures in the absence of divalent cations. SPE J. 15 (2), 341–348. https://doi.org/10.2118/121460-PA.
- Shin, S., Cho, Y.I., 1998. The effect of thermal degradation on the non-Newtonian viscosity of an aqueous polyacrylamide solution. KSME Int. J. 12, 267–273.

- https://doi.org/10.1007/BF02947171.
- Song, H., Pope, G.A., Mohanty, K.K., 2020. Thermal stability of acrylamide-based polymers at high temperature and high salinity. SPE Canada Heavy Oil Technical Conference. Calgary, Alberta, Canada. https://doi.org/10.2118/199921-MS.
- Supriya, B.S., Nagarja, P., Byrappa, K., 2015. Hydrothermal synthesis and characterization of carbon spheres using citric-acid-catalyzed carbonization of starch. E-Polymers 15 (3), 179—183. https://doi.org/10.1515/epoly-2015-0025.
- Taha, N.M., Lee, S., 2015. Nano Graphene Application Improving Drilling Fluids Performance. International Petroleum Technology Conference, Doha, Qatar. https://doi.org/10.2523/IPTC-18539-MS.
- Tan, Z., Yuan, S., Hong, M., et al., 2020. Mechanism of negative surface charge formation on biochar and its effect on the fixation of soil Cd. J. Hazard Mater. 384, 121370. https://doi.org/10.1016/j.jhazmat.2019.121370.
- Teherani, M.A., Popplestone, A., Guarneri, A., et al., 2007. Water-based drilling fluid for HP/HT applications. Int. Sympos. Oilfield Chem., Texas, USA. https://doi.org/10.2118/105485-MS.
- Thapliyal, V., Alabudulkarim, M.E., Whelan, D.R., et al., 2022. A concise review of the Raman spectra of carbon allotropes. Diam. Relat. Mater. 127, 109180. https://doi.org/10.1016/j.diamond.2022.109180.
- Titirici, M.M., Antonietti, M., 2010. Chemistry and materials options of sustainable carbon materials made by hydrothermal carbonization. Chem. Soc. Rev. 39, 103–116. https://doi.org/10.1039/B819318P.
- Titirici, M.M., 2013. Sustainable Carbon Materials from Hydrothermal Processes. John Wiley & Sons, Ltd.
- Wang, K., Jiang, G., Li, X., et al., 2020. Study of graphene oxide to stabilize shale in water-based drilling fluids. Colloid Surface A 606, 125457. https://doi.org/10.1016/j.colsurfa.2020.125457.
- Wang, T., Zhai, Y., Zhu, Y., et al., 2018. A review of the hydrothermal carbonization of

- biomass waste for hydrochar formation: process conditions, fundamentals, and physicochemical properties. Renew. Sustain. Energy Rev. 90, 223–247. https://doi.org/10.1016/j.rser.2018.03.071.
- Wang, Z., Ogata, H., Melvin, G.J.H., et al., 2017. Structural evolution of hydrothermal carbon spheres induced by high temperatures and their electrical properties under compression. Carbon 121, 426–433. https://doi.org/10.1016/ i.carbon.2017.06.003.
- Wu, C., Wei, C., Jin, X., et al., 2019. Carbon spheres as lubricant additives for improving tribological performance of polyetheretherketone. J. Mater. Sci. 54, 5127–5135. https://doi.org/10.1007/s10853-018-3177-4.
- Yang, B., Mao, J., Zhao, J., et al., 2019. Improving the thermal stability of hydrophobic associative polymer aqueous solution using a "triple-protection" strategy. Polymers (Basel) 11 (6), 949. https://doi.org/10.3390/polym11060949.
 Yu, S., Yang, X., Li, Q., et al., 2023. Breaking the temperature limit of hydrothermal
- Yu, S., Yang, X., Li, Q., et al., 2023. Breaking the temperature limit of hydrothermal carbonization of lignocellulosic biomass by decoupling temperature and pressure. Green Energy Environ. 8 (4), 1216–1227. https://doi.org/10.1016/ i.gee.2023.01.001.
- Zhang, M., Dong, Z., Fang, L., et al., 2023. Hydrothermal carbonization of size-controlled carbon microspheres from waste disposable towel with correlation analyze. Diam. Relat. Mater. 139, 110395. https://doi.org/10.1016/i.diamond.2023.110395.
- Zhong, H., Gao, X., Zhang, X., et al., 2020. Improving the shale stability with nanosilica grafted with hyperbranched polyethyleneimine in water-based drilling fluid. J. Nat. Gas Sci. Eng. 83, 103624. https://doi.org/10.1016/ j.jngse.2020.103624.
- Zhou, S.S., Song, J.J., Xu, P., et al., 2023. A review on tribology, characterization and lubricants for water-based drilling fluids. Geoenergy Sci. Eng. 229, 212074. https://doi.org/10.1016/j.geoen.2023.212074.